Isotopic Signatures of Methane Emissions from Dairy Farms in California's San Joaquin Valley

Valerie Carranza[1], Brenna Biggs[2], Deanne Meyer[3], Amy Townsend-Small[4], Ranga Rajan Thiruvenkatachari[1], Akula Venkatram[1], Marc Laurenz Fischer[5], and Francesca Hopkins[1]

[1]University of California, Riverside
[2]University of California, Irvine
[3]University of California, Davis
[4]University of Cincinnati
[5]Lawrence Berkeley National Laboratory (DOE)

November 23, 2022

Abstract

Since 2007, the global mole fraction of atmospheric methane (CH4) has steadily increased meanwhile the 13C/12C isotopic ratio of CH4 (expressed as δ13C-CH4) has shifted to more negative values. This suggests that CH4 emissions are primarily driven by biogenic sources. However, more in situ isotopic measurements of CH4 are needed at the local scales to identify which biogenic sources dominate CH4 emissions regionally. In California, dairies contribute a substantial amount of CH4 emissions from enteric fermentation and manure management. In this study, we present seasonal atmospheric measurements of δ13C-CH4 from dairy farms in the San Joaquin Valley of California. We used δ13C-CH4 to characterize emissions from enteric fermentation by measuring downwind of cattle housing (e.g., freestall barns, corrals) and from manure management areas (e.g., anaerobic manure lagoons) with a mobile platform equipped with cavity ring-down spectrometers. Across seasons, the δ13C-CH4 from enteric fermentation source areas ranged from -69.7 $\pm$ 0.6 per mil (ranged from -49.5 $\pm$ 0.1enteric CH4 suggest a greater than 10production groups in accordance with diet. Isotopic signatures of CH4 were used to characterize enteric and manure CH4 from downwind plume sampling of dairies. Our findings show that δ13C-CH4 measurements could improve the attribution of CH4 emissions from dairy sources at scales ranging from individual facilities to regions and help constrain the relative contributions from these different sources of emissions to the CH4 budget.

Isotopic Signatures of Methane Emissions from Dairy Farms in California's San Joaquin Valley

Valerie Carranza[1], Brenna Biggs[2], Deanne Meyer[3], Amy Townsend-Small[4], Ranga Rajan Thiruvenkatachari[5], Akula Venkatram[5], Marc L. Fischer[6], Francesca M. Hopkins[1]

[1] Department of Environmental Sciences & Environmental Dynamics and GeoEcology (EDGE) Institute, University of California, Riverside, CA 92521

[2] Department of Chemistry, University of California, Irvine, Irvine, CA 92697

[3] Department of Animal Science, University of California, Davis, Davis, CA 95616

[4] Departments of Geology and Geography, University of Cincinnati, Cincinnati, OH 45221

[5] Department of Mechanical Engineering, University of California, Riverside, CA 92521, USA

[6] Energy Technology Area, Lawrence Berkeley National Laboratory, Berkeley, California, USA

Corresponding author: Valerie Carranza (vcarr007@ucr.edu)

Key Points:

- Stable carbon isotopic signatures of methane emitted from manure lagoons were more enriched than methane from enteric fermentation
- Downwind plume sampling of stable carbon isotopic signatures of methane can be used to characterize enteric and manure methane
- Isotopic signatures of methane varied between different cattle production groups in accordance with diet

Keywords: methane, greenhouse gas emissions, carbon isotopes, dairy, source apportionment

ABSTRACT

Since 2007, the global mole fraction of atmospheric methane (CH_4) has steadily increased meanwhile the $^{13}C/^{12}C$ isotopic ratio of CH_4 (expressed as $\delta^{13}C_{CH4}$) has shifted to more negative values. This suggests that CH_4 emissions are primarily driven by biogenic sources. However, more in situ isotopic measurements of CH_4 are needed at the local scales to identify which biogenic sources dominate CH_4 emissions regionally. In California, dairies contribute a substantial amount of CH_4 emissions from enteric fermentation and manure management. In this study, we present seasonal atmospheric measurements of $\delta^{13}C_{CH4}$ from dairy farms in the San Joaquin Valley of California. We used $\delta^{13}C_{CH4}$ to characterize emissions from enteric fermentation by measuring downwind of cattle housing (e.g., freestall barns, corrals) and from manure management areas (e.g., anaerobic manure lagoons) with a mobile platform equipped with cavity ring-down spectrometers. Across seasons, the $\delta^{13}C_{CH4}$ from enteric fermentation source areas ranged from -69.7 ± 0.6 per mil (‰) to -51.6 ± 0.1‰ while the $\delta^{13}C_{CH4}$ from manure lagoons ranged from -49.5 ± 0.1‰ to -40.5 ± 0.2‰. Measurements of $\delta^{13}C_{CH4}$ of enteric CH_4 suggest a greater than 10‰ difference between cattle production groups in accordance with diet. Isotopic signatures of CH_4 were used to characterize enteric and manure CH_4 from downwind plume sampling of dairies. Our findings show that $\delta^{13}C_{CH4}$ measurements could improve the attribution of CH_4 emissions from dairy sources at scales ranging from individual facilities to regions and help constrain the relative contributions from these different sources of emissions to the CH_4 budget.

Plain Language Summary

Methane emissions from livestock production are an important part of the global methane budget. However, more measurements of carbon isotopes of methane are needed to help constrain the relative contribution of methane sources regionally. In this study, we measured

carbon isotopes of methane at dairy farms in California, the leading dairy-producing state in the United States. Different areas of the dairy farm had distinct methane generation processes, reflected in the isotopic signatures of methane that were emitted. Methane from manure lagoons was more enriched in the heavier of carbon's two stable isotopes, carbon-13, than methane from enteric fermentation across seasons at a dairy farm. Isotopic signatures of methane were relatively invariant across seasons, particularly from manure lagoons. In addition, enteric methane from different cattle production groups had distinct isotopic signatures of methane that are likely dependent on diet composition. Isotopic signatures can also be used to apportion methane emissions from both enteric fermentation and anaerobic manure lagoons by taking samples downwind of dairy farms. This can help constrain the relative contributions from these different sources of emissions to the methane budget, as well as track the effectiveness of mitigation strategies by estimating the contribution of sources.

1 Introduction

Methane (CH_4) is the second most important anthropogenic greenhouse gas after carbon dioxide and is increasingly becoming a critical priority for near-term climate action, given its relatively short lifetime and substantial potential for rapid mitigation (United Nations, 2021). Over the last several decades, the growth rate of atmospheric CH_4 has significantly changed, reaching stable zero growth from 1999 to 2006, followed by an increase beginning 2007 (Dlugokencky et al., 1998; Nisbet et al., 2014). This rise in the global mole fraction of atmospheric CH_4 has been the subject of several studies that focus on explaining this phenomenon, without a definitive explanation. A rise in CH_4 emissions could be indicative of changes in total emissions from various sources, including from biogenic, thermogenic, and pyrogenic CH_4 and/or a decrease in the atmospheric sink of CH_4 (Naus et al., 2019; Nisbet et al., 2016; Rigby et al., 2017; Turner et al., 2017; Worden et al., 2017).

The isotopic signature of CH_4 is an important tool to diagnose the source of this increase in CH_4 (Dlugokencky et al., 2011). The global stable carbon isotope ratio of atmospheric CH_4, expressed as $\delta^{13}C_{CH4}$, has shifted towards more negative values simultaneously with the rise of the atmospheric mole fraction of CH_4 (Schaefer et al., 2016). Recent isotopic evidence suggests that this rise in CH_4 is likely dominated by increased emissions of biogenic CH_4, which are more depleted in ^{13}C relative to fossil and pyrogenic CH_4 sources (Nisbet et al., 2016). Possible biogenic sources responsible for the rise in atmospheric CH_4 include ruminants, rice paddies, and wetlands, among others, with $\delta^{13}C_{CH4}$ estimates of about -60‰ for C3-fed ruminants and about -50‰ for C4-fed ruminants (Dlugokencky et al., 2011; Nisbet et al., 2016; Schaefer et al., 2016). Previous work have shown that isotopic signatures of CH_4 emitted by enteric fermentation depend on the carbon isotopic ratio of diet composition, driven by the proportion of plants with C3 and C4 photosynthetic pathways (Metges et al., 1990; Levin et al., 1993; Schulze et al., 1998; Bilek et al., 2001; Schwietzke et al., 2016). However, we lack sufficient in situ isotopic characterization of CH_4 at the local level to identify the location and type of biogenic sources that dominate the current rise in global CH_4 emissions (Nisbet et al., 2019). Even at local to regional scales, the budgets of both CH_4 and its stable carbon isotope remain uncertain (Townsend-Small et al., 2012). Improved knowledge is particularly important for ensuring effective mitigation of CH_4 at scales where policies to reduce CH_4 are being enacted (Hopkins et al., 2016a).

In California, there are statewide efforts underway to reduce CH_4 emissions, but it remains challenging to accurately monitor progress given the large inconsistencies between atmospheric observations and greenhouse gas inventories (Jeong et al., 2013; Duren et al., 2019). Atmospheric observations have inferred higher CH_4 emissions than reported in GHG inventories at the statewide and regional levels and from individual sectors, including dairies (Cui et al., 2017; Jeong et al., 2016; Miller et al., 2013; Trousdell et al., 2016; Wecht et al., 2014). However, there is little information about the processes that produce this apparent discrepancy. The California Air Resources Board (CARB) GHG inventory estimates that dairies contribute about half of statewide CH_4 emissions, with contributions from enteric fermentation by ruminant gut microbes and manure managed in anaerobic conditions. However, these estimates are based on emission factors derived from a few pilot and lab-scale studies conducted outside of California and thus likely not representative of California's climate and unique biogeography (Owen & Silver, 2015). Given that mitigation practices are targeted towards the biogeochemical and management processes that produce CH_4, new tools for source apportionment and process understanding are required. Stable isotopes of CH_4 may be a promising way forward.

The few studies that have measured isotopic signatures of CH_4 from dairies in California were done in the Los Angeles Basin. Townsend-Small et al. (2012) investigated the isotopic signature of major sources of CH_4 in the in the Los Angeles megacity, and found that isotopic values of $\delta^{13}C_{CH4}$ from fields applied with cow manure were characterized by values between -62.1 per mil (‰) to -59.2‰, whereas $\delta^{13}C_{CH4}$ of manure biofuel from a manure digester facility ranged from -52.4‰ to -50.3‰. Cow breath, on the other hand, had more depleted $\delta^{13}C_{CH4}$ source signatures between -64.6‰ and -60.2‰. A more recent study by Viatte et al. (2017) measured isotopic signatures of $\delta^{13}C_{CH4}$ from the largest dairy farms in Southern California, and observed values between -65‰ to -45‰, attributing the most depleted observations to enteric fermentation.

In Europe, previous research has shown that $\delta^{13}C_{CH4}$ signatures vary dependent on the type of dairy manure storage. In Heidelberg, Germany, Levin et al., (1993) observed more enriched $\delta^{13}C_{CH4}$ from manure piles (-45.5±1.3‰) and a biogas generator (-51.8±2.8‰) than liquid manure (-73.9±0.7‰). Two recent studies used mobile surveys to measure $\delta^{13}C_{CH4}$ in Europe. In Germany, Hoheisel et al. (2019) conducted mobile measurements to determine $\delta^{13}C_{CH4}$ signatures around Heidelberg and in North Rhine-Westphalia. The $\delta^{13}C_{CH4}$ signatures ranged from -66.0‰ to -40.3‰ for three dairy farms with biogas plants. More enriched $\delta^{13}C_{CH4}$ signatures were observed from plumes downwind of the biogas plant relative to plumes downwind of the animal housing. In Northern England, Lowry et al., (2020) found that methane plumes downwind of dairy farms had $\delta^{13}C_{CH4}$ signatures from -67‰ to -58‰. Atmospheric measurements downwind of manure piles were more enriched in $^{13}C_{CH4}$ with values close to -50‰ relative to cow breath, which were close to -70‰. Isotopic endmembers were variable downwind of animal housing dependent on the cattle population and amount of manure waste present. In general, CH_4 from barns with fewer cows and more manure waste were more enriched in ^{13}C.

In this study, we present seasonal atmospheric measurements of $\delta^{13}C_{CH4}$ from dairy farms located in the San Joaquin Valley, California, where 91% of the state's dairy herd resides (Mullinax et al., 2020). Our primary objective was to measure $\delta^{13}C_{CH4}$ emitted from anaerobic manure lagoons and enteric fermentation source areas across seasons. Our second objective was to use $\delta^{13}C_{CH4}$ source signatures from enteric fermentation and anaerobic lagoons to identify the dominant source responsible for CH_4 hotspots detected from downwind plume sampling of other dairies in the region. We hypothesized that the $\delta^{13}C_{CH4}$ signatures from dairy anaerobic manure lagoons and enteric fermentation can be used to apportion CH_4 emissions between these two dairy farm source processes. These isotopic signatures can help contribute to the body of knowledge that aims to resolve the CH_4 budget in California and globally.

2 Methodology

2.1 Study Site

Ground-based mobile measurements were collected at a dairy in Tulare County (San Joaquin Valley), California, in the fall, spring, summer, and winter seasons from 2018 to 2020. Hereafter, we will refer to this dairy as the reference test site farm. Figure 1 shows a schematic of the reference test site farm layout. The reference test site has on average 3070 milking cows that spend most of their time in freestall barns, with an additional ~400 dry cows and ~3000 heifers that are primarily in open lots (corrals). Manure waste is handled using a combination of wet and dry manure management practices (Meyer et al., 2019). Wet manure management is used for waste deposited in the freestall barns, where manure waste is flushed from barn floors and diverted to a processing pit. Wastewater from the milking parlor also enters the processing pit. Processing pit water is reused to flush lanes or is pumped over stationary inclined screen (manure separator). A manure separator then removes coarser solids (17% of total solids) from liquid effluent, which gravity flows into cell 1. The liquid manure navigates from separation cell 1, cell 2, the primary lagoon, and finally into a holding pond via gravity, decreasing the content of suspended volatile solids through anaerobic decomposition and settling as it moves from one component to the next. Water waste from the holding pond is later used as irrigation water for cropland. Hereafter, manure lagoons refer to cell 1, cell 2, primary lagoon, and the holding pond. Dry manure management refers to the fraction of waste that is separated from the liquid waste stream, which is spread out on the ground and solar dried. Once dry, this manure is distributed into freestall beds (bedding) or stacked and covered in the dry bedding. The primary forages are wheat and corn preserved as silage. Silage piles are covered with a double layer of plastic.

The feed composition for different seasons was obtained by weighing each feed ingredient as it was included into the mixer wagon. All weights were transferred electronically to feed management software (VAS FeedWatch). FeedWatch data were retrieved once monthly for ingredient identification, quantity fed per pen, pen population and dry matter composition. Each ingredient was identified as C3 or C4 except for distiller's grain, which could be a changing combination of C3 and C4 sources. Sum of dry weights by pen for C3, C4, distillers feeds were calculated. The feed composition by cattle production group is presented in Table 3.

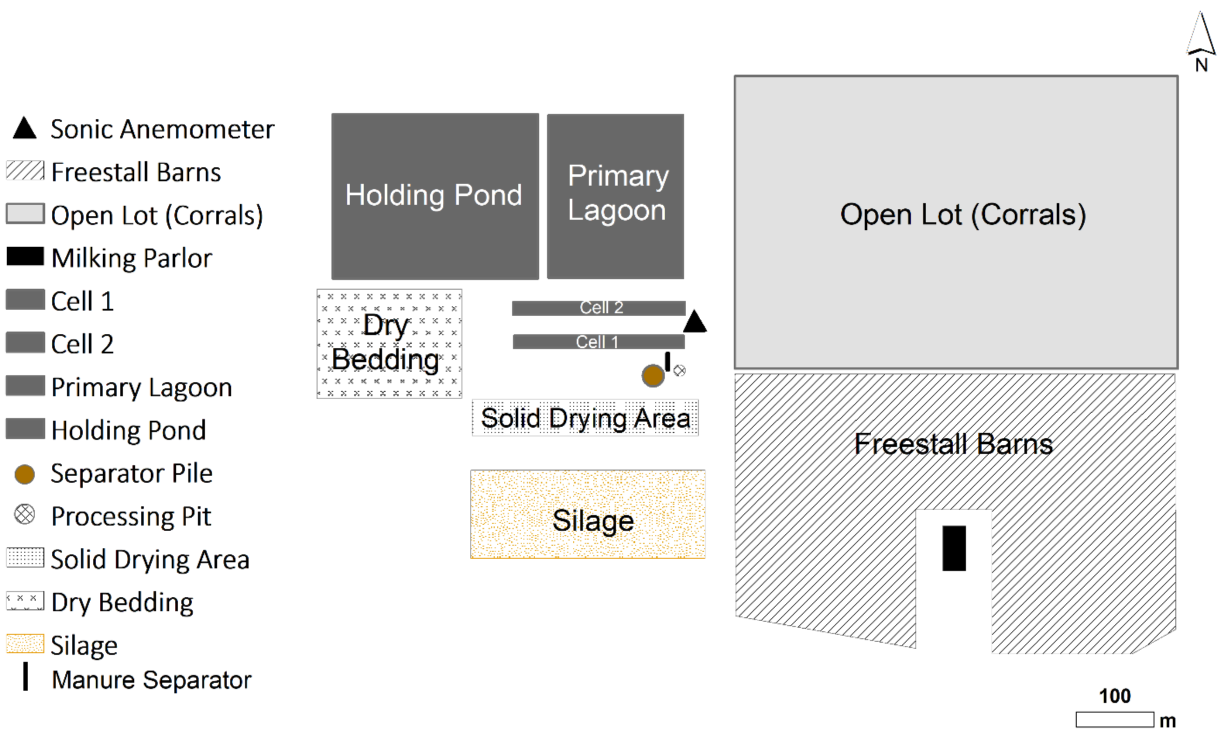

Figure 1. Facility layout and location of sonic anemometer on the reference test site of the San Joaquin Valley, California.

We also made measurements at other dairies within a 10 x 10 km region of agricultural land in the same county, which includes additional dairy farms, beef feedlots, poultry farms, and a landfill that are also emitting methane (Figure 2). Other potential sources of emissions surround the region, including a wetland, plugged and abandoned oil and gas wells that are permanently sealed, and a wastewater treatment plant (Figure 2). Residential land is primarily located south of the region and contains an extensive natural gas pipeline network.

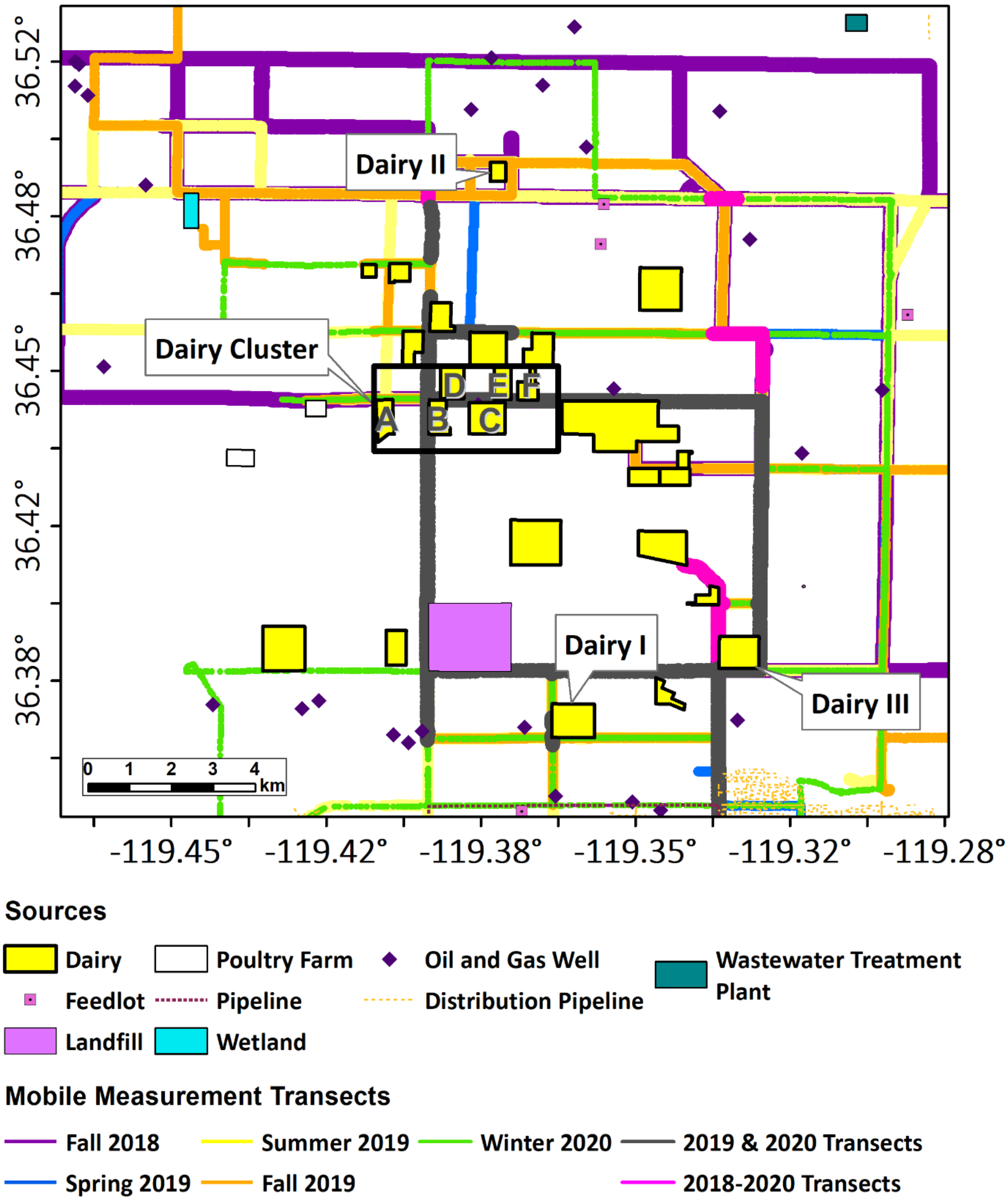

Figure 2. Mobile measurements routes in Tulare County region of the San Joaquin Valley, California. The symbols indicate the major known CH_4 sources in this agricultural region. The location of dairies sampled across multiple seasons are specified as Dairy I, Dairy II, Dairy III,

and Dairy Cluster (A-F). Mobile measurement routes are colored by different seasonal campaigns. The pink lines show routes that were sampled in all 2018-2020 transects and the black lines show routes that were sampled in all 2019 and 2020 transects.

2.2 Mobile Platform and Micrometeorological Measurements

Continuous measurements of greenhouse gases and pollutants were collected using a mobile platform (Thiruvenkatachari et al., 2020), consisting of analyzers using the Cavity Ring-Down Spectroscopy (CRDS) technique (Picarro G2210-*i* and Picarro G2401, Picarro, Inc., Santa Clara, CA, USA), global satellite positioning unit (GPS 16X, Garmin Ltd., Olathe, KS, USA) to record geolocation and vehicle speed, 2-D sonic anemometer (METSENS500, Campbell Scientific, Inc., Logan, UT, USA) to measure wind direction, wind speed, air temperature and relative humidity, and calibration tanks. The following trace gas species were continuously measured from air drawn in at an inlet with a height of 2.87 m: CH_4, $\delta^{13}C_{CH4}$, carbon dioxide (CO_2), carbon monoxide (CO), ethane (C_2H_6). Reported trace gas mole fractions and isotope ratios were corrected using low and high custom gas mixtures that were measured before and after each measurement period. These gas mixtures contained all the species of interest and were tied to the scale set by the NOAA Global Monitory Division (GMD) by measurement against NOAA certified tanks. Isotopic standards were tied to the Vienna Pee Dee Belemnite (VPDB) scale. Methane isotope measurements with the Picarro G2210-*i* were further validated and corrected for instrument drift with standards ranging from -23.9‰ to -68.6‰ in the laboratory.

Micrometeorological measurements were collected at the reference test site each season, with a 3-D sonic anemometer (CSAT3, Campbell Scientific, Inc.) mounted on a stationary tower near the manure lagoons (Figure 1). Measurements were made at two heights, 2.4 m and 11 m, at a frequency of 20 Hz. For the purposes of our analysis, we only used meteorological data from the 2.4 m tower.

On January 15th, 2020, we used a cuboid chamber (17.8 cm height and 28.0 cm width) made of clear PVC to isolate and measure $\delta^{13}C_{CH4}$ from freestall barns and static manure piles from the solid drying area (Litvak et al., 2014). The chamber was placed on the freestall barn or manure pile surface and connected to the gas analysis system of the mobile platform with Synflex tubing. For each sample, we collected measurements for ten minutes. We also measured $\delta^{13}C_{CH4}$ from the breath of milking cows, dry cows, heifers, bull calves, and calves in hutches by holding Synflex tubing connected to the mobile platform gas analysis system near the mouths of cows (Townsend-Small et al., 2012). We measured within 16 cm of milking and dry cows, ~1 m from heifers and bull calves, and ~10 m from calves in hutches.

2.2 Data Processing

Several corrections to observations were applied for each measurement period. First, observations collected from different instruments were cross-correlated and synchronized to local time (Hopkins et al., 2016b). Offsets were recorded between local time and each instrument's internal clock, which were then used to correct data prior to performing the cross-correlation method. Second, a correction was applied based on the lag time between the inlet and instrument reading. Third, trace gas mole fraction and $\delta^{13}C_{CH4}$ observations were corrected by applying a correction factor from calibrations performed before and after each measurement period. Observations were averaged over 1-s intervals.

2.3 Whole Air Samples and Continuous Mobile Laboratory Measurements

We compared measurements of $\delta^{13}C_{CH4}$ using our mobile laboratory sampling technique using CRDS with analysis of whole-air samples collected at the same time and then analyzed with standard Isotope Ratio Mass Spectrometry (IRMS). Five whole-air samples of atmospheric CH_4 were collected in preconditioned and evacuated 2-L stainless steel canisters with bellow valves, over a period of about one minute (Blake et al., 1994; Colman et al., 2001). Whole-air samples were collected at the same height of the mobile laboratory inlet. The canisters were first processed by University of California, Irvine for chemical analysis, and a subsample was then sent to the University of Cincinnati for isotopic analysis with IRMS using a method described in detail by Yarnes (2013). Over the course of the same time intervals, the mobile laboratory continuously measured $\delta^{13}C_{CH4}$ with the CRDS instrument. We found no statistically significant difference between individual CRDS and IRMS samples using a Student's t-test (Table 1); the differences between $\delta^{13}C$ measured by IRMS and CRDS were always less than the uncertainties of each technique alone. These findings suggest that $\delta^{13}C_{CH4}$ measurements by the mobile laboratory CRDS technique is comparable to the standard IRMS method.

Table 1. Samples Collected by the Mobile Platform Using the CRDS and IRMS Technique.

Date	Local Time[a]	Source Type[b]	IRMS δ^2H-CH_4 (‰)[c]	IRMS δ^{13}C-CH_4 (‰)[c]	Average CRDS δ^{13}C-CH_4 (‰)[d]	n[e]	p value
March 25, 2019	13:37:50 - 13:38:50	Cell 1	-326 ± 4	-42.91 ± 0.23	-43.27 ± 0.18	34	0.06
March 25, 2019	18:37:30 - 18:38:30	Primary lagoon	-263 ± 4	-50.13 ± 0.23	-49.90 ± 0.18	44	0.22
March 26, 2019	7:52:05 - 7:53:05	Freestall barns	-280 ± 4	-54.16 ± 0.23	-54.21 ± 0.18	46	0.77
March 26, 2019	8:12:30 - 8:13:30	Corrals	-277 ± 4	-52.07 ± 0.23	-52.01 ± 0.18	45	0.74
March 26, 2019	9:12:30 - 9:13:30	Landfill	-245 ± 4	-49.21 ± 0.23	-49.03 ± 0.18	47	0.32

[a] Time interval for CRDS measurements. IRMS samples were also instantaneously collected within this time interval.

[b] All source types were at reference test site except the landfill (Figure 2).

[c] Precision of the IRMS technique is reported.

[d] Standard error of the average of standard gas measurements are reported.

[e] Number of CRDS observations that were averaged.

We conducted a dilution experiment to analyze the precision of $\delta^{13}C_{CH4}$ sampled with the CRDS instrument at varying CH_4 levels similar to what we observed during downwind plume sampling of other dairies in the region. Following a similar method by Miles et al. (2018), a high gas standard with 20.1 ppm CH_4 and δ^{13}C-CH_4 of -44.35‰ (traceable to the scale set by the NOAA GMD by measurement against NOAA certified tanks) was mixed with zero air using a mass flow controller (MC-20SLPM-D-SV and MCS-100SCCM-D-PCV03, Alicat Scientific, Inc.). The mass flow controllers were used to direct isotopic calibration standard tank into a mixing volume at 20 sccm (standard cubic centimeter per minute) and mixed with zero CH_4 air at 203.3, 181.0, 140.0, 114.00, 20.2 and 13.5 sccm to create target CH_4 mole fractions of 1.8, 2.0 , 2.5, 3.0, 10.0 and 12.0 ppm, respectively. To compare with the time interval used to average regional measurements, the final 15 seconds of data for each dilution were averaged to evaluate the precision of the instrument. The standard error of the δ^{13}C-CH_4 collected during these tests increased with decreasing mole fractions. The $\delta^{13}C$ end-member (-43.52‰) from the data collected was within 0.83‰ of the isotopic value of calibration standard tank.

2.4 Farm-scale Analysis

Sources of CH_4 emissions at the reference test site farm were identified by categorizing atmospheric observations based on proximity to the emission source and wind direction. To evaluate $\delta^{13}C_{CH4}$ from biogenic sources at the farm scale, observations with $CH_4 \leq 30$ ppmv were selected and averaged by 1-min intervals to minimize uncertainty according to the performance standards of the instrument. For each source, $\delta^{13}C_{CH4}$ and the corresponding standard errors were estimated as the y-intercept from a weighted linear regression of the inverse of the atmospheric CH_4 mole fraction and $\delta^{13}C_{CH4}$ (i.e., Keeling plot) (Keeling, 1958; Pataki et al., 2003). Keeling plots were generated for each dairy farm source (i.e., manure lagoons, corrals, and freestall barns) by applying a weighted linear regression with errors in both the independent and dependent variables (i.e., *x*-data: CH_4^{-1} and *y*-data: $\delta^{13}C_{CH4}$) based on the York et al. (2004) method (Thirumalai et al., 2011). To exclude CH_4 emissions from fossil-fuel sources, such as from vehicles, we omitted CH_4 observations that had corresponding excess C_2H_6 values > 0.1 ppm (0.02% of reference test site farm measurements) and excess CO values > 500 ppb, the 99th percentile from all regional transects (Miller et al., 2015). We define excess C_2H_6 and excess CO as mole fractions above the minimum C_2H_6 and CO observations for each dairy farm source. At the reference test site, no excess CO measurements above this threshold were detected. For the inverse of CH_4, the uncertainty was defined as the mean of the standard errors from the 1-min averaged observations in the weighted linear regression. For $\delta^{13}C_{CH4}$ observations, we first evaluated the mean of the standard errors from the 1-min averaged observations against the standard error from 1-min averages of the standard gas run. Then, we selected the largest standard error of the two as the corresponding uncertainty. In this study, the $\delta^{13}C_{CH4}$ values reported hereafter are referring to the $\delta^{13}C_{CH4}$ end-members derived from Keeling plots.

2.5 Downwind Plume Sampling Analysis

Isotopic signatures of CH_4 were classified into the following two categories: Dairy Cluster (dairies A-F) or isolated dairy farms (Dairy I, Dairy II, Dairy III), where there were no major potential sources of CH_4 within at least 2 km from the dairy farm (Figure 2). We used 15-s averaged observations to detect CH_4 hotspots, defined as locations with CH_4 levels exceeding 350 ppb above local background. We exclude potential CH_4 emissions from fossil fuel sources using the same C_2H_6 and CO criteria as described above. For each season, we then identified hotspots of CH_4 downwind of dairy farms and derived the $\delta^{13}C$ end-members with a Keeling plot, using the method described in section 2.4. To ensure the method described in section 2.4 is appropriate for the lower mole fractions observed from downwind sampling of other dairies in the region, we compared the $\delta^{13}C$ end-members using the standard error from the CH_4 dilution experiment described in section 2.3 against the standard error selected using the method described in section 2.4. There was no statistically significant difference between $\delta^{13}C$ end-members using Welch's t-test. Thus, to be consistent with analysis at the farm-scale, the method described in section 2.4 was selected to obtain source $\delta^{13}C$ end-members from downwind plume sampling of other dairies.

Isotope mixing equations from Fry (2006) were used to estimate the fractional contribution of the two CH_4 sources, enteric fermentation source areas and manure lagoons, from CH_4 hotspots. We averaged the isotopic signatures of cow breath measurements ($\delta_{enteric}$) from milking cows, dry cows, heifers, bull calves, and calves in hutches from the winter 2020 measurements from the reference test site (-61.06 ± 0.27‰). We also averaged the manure lagoon isotopic signatures, δ_{manure}, observed at the reference test site (-45.13 ± 0.41‰). The following equation was used to estimate the fraction of enteric methane emissions,

$$f_{enteric} = (\delta_{observation} - \delta_{manure}) / (\delta_{enteric} - \delta_{manure})$$

where $f_{enteric}$ is the fraction of enteric methane from the total sum of two sources and $\delta_{observation}$ is the isotopic signature of the CH_4 hotspot. Uncertainties were calculated by propagation of error.

To further characterize CH_4 hotspots, we used a Eulerian numerical (EN) dispersion model to identify the CH_4 flux footprint, which is the upwind area where CH_4 emissions measured by the mobile platform were generated (refer to details in Thiruvenkatachari et al., 2020). For this study, the EN model identified which dairy farm areas contributed the most to the atmospheric CH_4 observations. We applied a roughness length of 0.002 m in the EN model. The dairy farm areas were divided into smaller sources by a 5 m grid.

3 Results

3.1 Source-scale Isotopic Signatures of CH_4 Measured at a Single Farm

Different sources of CH_4 emissions of the dairy farm had distinct isotopic signatures of CH_4 that were relatively invariant across seasons (Figure 3, Table 2). The $\delta^{13}C_{CH4}$ signatures from enteric fermentation source areas were more depleted than CH_4 from manure lagoons. The $\delta^{13}C_{CH4}$ from animal housing areas ranged from -69.7 ± 0.6‰ to -51.6 ± 0.1‰, whereas the $\delta^{13}C_{CH4}$ from manure lagoons ranged from -49.5 ± 0.1‰ to -40.5 ± 0.2‰. Methane emissions from freestall barns had heavier $\delta^{13}C_{CH4}$, with values ranging from -59.9 ± 0.2‰ to -51.6 ± 0.1‰. Meanwhile, corrals exhibited the most depleted $\delta^{13}C_{CH4}$, ranging from -69.7 ± 0.6‰ to -55.5 ± 0.5‰. Specifically, there were seasonal differences in isotopic signatures from manure lagoons. The most enriched $\delta^{13}C_{CH4}$ from manure lagoons was observed in January 2020 (-40.5 ±

0.2‰) relative to other seasons, such as in June 2019 (-49.5 ± 0.1‰) and September 2019 (-46.69 ± 0.02‰). Freestall barns and corrals displayed a relatively larger range, but, notably, the heaviest $\delta^{13}C_{CH4}$ was observed in September 2018 (freestall barns: -52.8 ± 0.1‰) and January (freestall barns: -51.6 ± 0.1‰), with the most depleted $\delta^{13}C_{CH4}$ observed in September 2018 (corrals: -69.7 ± 0.6‰).

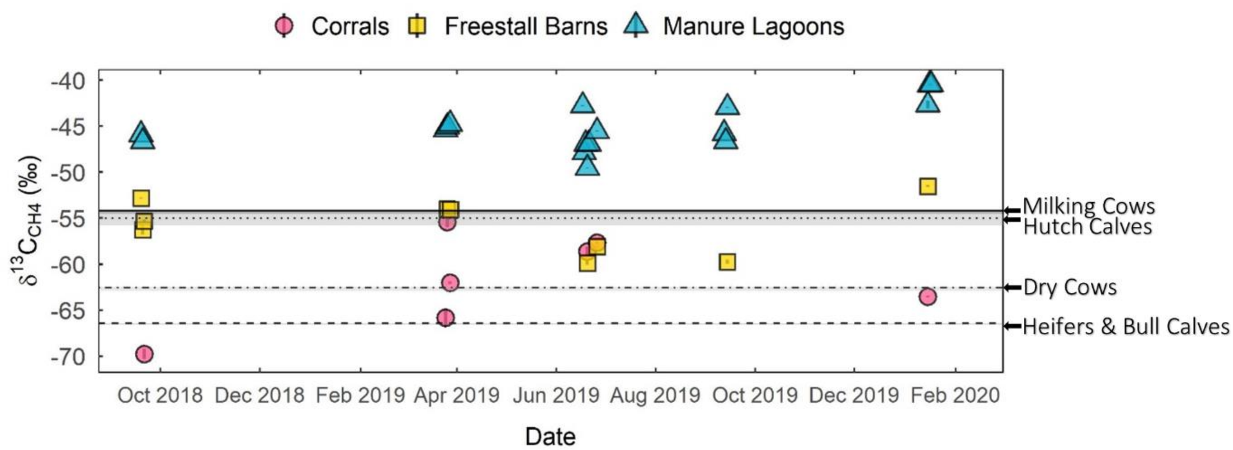

Figure 3. Seasonal $\delta^{13}C_{CH4}$ isotopic signatures from different CH_4 source areas on the reference test site farm (corrals, freestall barns, and manure lagoons). Each symbol represents the $\delta^{13}C_{CH4}$ isotopic signature derived from Keeling plots. The lines and shaded regions represent the $\delta^{13}C_{CH4}$ isotopic signatures (lines) and associated standard errors (shaded regions) of cow breath by cattle type during the winter 2020 campaign (Figure 4).

Table 2. Seasonal $\delta^{13}C_{CH4}$ Isotopic Signatures at a Dairy Farm (i.e., Reference Test Site).

Season	Date	Source	$\delta^{13}C_{CH4}$ (‰)[a]
	September 19, 2018	Freestall Barns	-52.8 ± 0.1
Fall	September 20, 2018	Freestall Barns	-56.2 ± 0.5
	September 21, 2018	Freestall Barns	-55.4 ± 0.2
Spring	March 26, 2019	Freestall Barns	-54.1 ± 0.1
	March 28, 2019	Freestall Barns	-54.0 ± 0.1

Summer	June 20, 2019	Freestall Barns	-59.9 ± 0.2
	June 26, 2019	Freestall Barns	-58.2 ± 0.1
Fall	September 14, 2019	Freestall Barns	-59.8 ± 0.2
Winter	January 15, 2020	Freestall Barns	-51.6 ± 0.1
Fall	September 21, 2018	Corrals	-69.7 ± 0.6
Spring	March 25, 2019	Corrals	-65.7 ± 1.0
	March 26, 2019	Corrals	-55.5 ± 0.5
	March 28, 2019	Corrals	-62.1 ± 0.1
Summer	June 20, 2019	Corrals	-58.6 ± 0.5
	June 26, 2019	Corrals	-57.6 ± 0.2
Winter	January 15, 2020	Corrals	-63.5 ± 0.1
Fall	September 19, 2018	Manure Lagoons	-46.02 ± 0.03
	September 20, 2018	Manure Lagoons	-46.75 ± 0.04
Spring	March 25, 2019	Manure Lagoons	-45.48 ± 0.02
	March 26, 2019	Manure Lagoons	-45.2 ± 0.1
	March 28, 2019	Manure Lagoons	-44.9 ± 0.1
Summer	June 17, 2019	Manure Lagoons	-42.9 ± 0.1
	June 18, 2019	Manure Lagoons	-47.99 ± 0.03
	June 19, 2019	Manure Lagoons	-47.03 ± 0.01
	June 20, 2019	Manure Lagoons	-49.5 ± 0.1
	June 21, 2019	Manure Lagoons	-46.94 ± 0.03
	June 26, 2019	Manure Lagoons	-45.5 ± 0.1
Fall	September 12, 2019	Manure Lagoons	-45.80 ± 0.02
	September 13, 2019	Manure Lagoons	-46.69 ± 0.02
	September 14, 2019	Manure Lagoons	-43.0 ± 0.1
Winter	January 15, 2020	Manure Lagoons	-42.7 ± 0.4
	January 16, 2020	Manure Lagoons	-40.5 ± 0.2
	January 17, 2020	Manure Lagoons	-40.5 ± 0.1

[a] Standard errors are reported for $\delta^{13}C_{CH4}$ isotopic signatures derived from Keeling plot analyses. All *p* values are <0.001, except on September 14, 2019 for Freestall Barns (*p* value = 0.01) and January 15, 2020 for Manure Lagoons (*p* value = 0.85)

Differences in the isotopic signatures from CH_4 emissions generated from the freestall barns and corrals may be explained by the types of cattle housed in each area. To further explore this, we conducted isolated breath measurements of different cattle production groups during the winter season and evaluated their diet composition across seasons. Freestall barns only house milking cows and cows within a few days of parturition, while corrals house milk-fed calves in hutches (hereafter, hutch calves), heifers, bull calves, and dry cows (i.e., non-lactating cows). As shown from the Keeling plots in Figure 4, the breath of milking cows (-54.2 ± 0.2‰) and hutch calves (-55.0 ± 1.7‰) were more enriched in $\delta^{13}C_{CH4}$ relative to dry cows (-62.6 ± 0.3‰) and heifers and bull calves (-66.4 ± 0.2‰).

We used feed data collected at our reference test site farm to interpret the variations in $\delta^{13}C$ of CH_4 emited from cattle in corrals and freestall barns at the reference test site farm. We found that the types of cattle housed in each area were each fed a distinct type of feed, consisting of C3, C4, or distiller's dried grains of unknown composition (DDG) (Table 3). In all seasons, milking cows were fed a mixture consisting primarily of C3 (36-43%) and C4 feeds (50-58%), with a small percentage of DDG (5-8%). Hutch calves were milk-fed and also fed a mixture of C3, C4, and DDG feed, but with a larger percentage of DDG (27-45%)—the diet composition for hutch calves was more variable depending on the season. Bull calves were fed a wide range of C3 (12-45%), C4 (12-66%), and DDG (22-43%) feed depending on the month. In contrast, dry cows and heifers were predominately fed a C3 diet (85-100%) with a small percentage of DDG (0-15%). Given that isotopic measurements of substrates were outside the scope of this study, we assumed that C4 feed had a $\delta^{13}C$ of -12.24 ± 0.34‰ and C3 feed had a $\delta^{13}C$ of -23.61‰ based on reported $\delta^{13}C$ of maize and wheat in Chang et al. (2019). For DDG, we assumed an equal mixture of C3 and C4 feed, resulting in a $\delta^{13}C$ of -17.93 ± 0.34‰. To estimate the expected $\delta^{13}C_{CH4}$ for different cattle production groups at the reference test site, we used the linear regression equation derived from the empirical relationship between $\delta^{13}C_{diet}$ and $\delta^{13}C_{CH4}$ from enteric fermentation of ruminants in Chang et al. (2019) ($\delta^{13}C_{CH4} = 0.91 \times \delta^{13}C_{diet} - 43.49‰$, with the standard errors of the intercept and slope being 2.86‰ and 0.12‰, respectively). Based on these assumptions, milking cows and hutch calves are projected to emit more enriched $\delta^{13}C_{CH4}$ values relative to other cattle production groups (Table 3). Although this pattern generally agrees with our study's $\delta^{13}C_{CH4}$ measurements from enteric fermentation source areas, our $\delta^{13}C_{CH4}$ measurements were often more enriched than expected. The $\delta^{13}C_{CH4}$ from animal housing is likely impacted by isotopically enriched CH_4 from manure deposited in corrals and freestall barns.

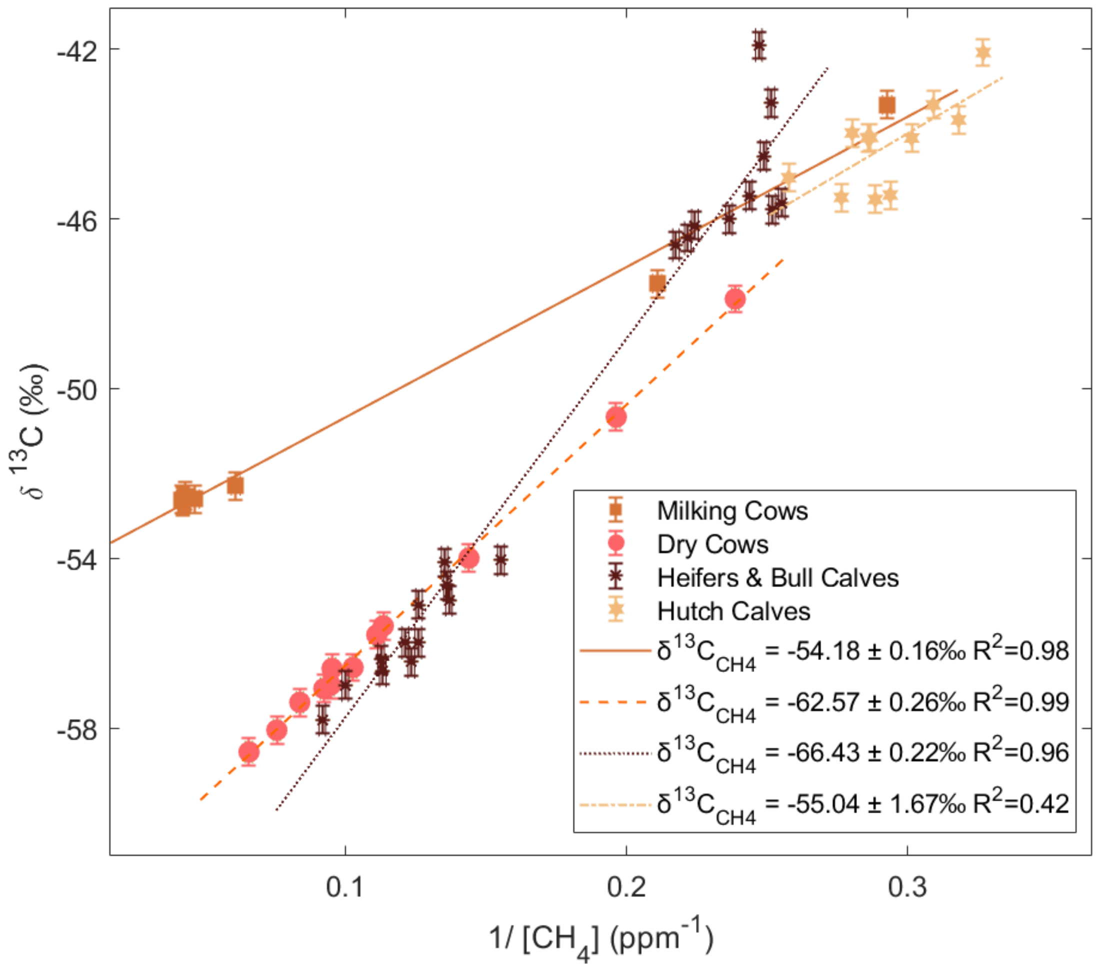

Figure 4. Keeling plot of $1/CH_4$ concentration versus $\delta^{13}C$ isotope measurements of CH_4 from cow breath on January 15th, 2020. Different cattle types and their Keeling intercepts are shown with different colors in the key.

Table 3. Feed Composition at Reference Test Site Farm.

Cow Type	Month	C4 (%)	C3 (%)	DDG (%)	Estimated $\delta^{13}C_{CH4}$ (‰)[a]
Milking Cows	Oct 2018	42	50	8	-60.22 ± 2.90

	Jan 2019	36	57	7	-60.89 ± 2.90
	Mar 2019	36	58	6	-60.94 ± 2.90
	Jun 2019	37	57	6	-60.84 ± 2.90
	Sep 2019	43	50	5	-60.17 ± 2.90
Dry Cows	Oct 2018	0	100	0	-64.98 ± 2.90
	Jan 2019	0	100	0	-64.98± 2.90
	Mar 2019	0	100	0	-64.98 ± 2.90
	Jun 2019	0	100	0	-64.98 ± 2.90
	Sep 2019	0	100	0	-64.98 ± 2.90
Heifers	Oct 2018	0	87	13	-64.30 ± 2.90
	Jan 2019	0	86	14	-64.25 ± 2.90
	Mar 2019	0	90	14	-64.28 ± 2.90
	Jun 2019	0	92	15	-64.25 ± 2.90
	Sep 2019	0	85	15	-64.20 ± 2.90
Bull Calves	Oct 2018	45	12	43	-58.09 ± 2.90
	Jan 2019	23	51	26	-61.25 ± 2.90
	Mar 2019	20	55	25	-61.61 ± 2.90
	Jun 2019	17	59	24	-61.97 ± 2.90
	Sep 2019	12	66	22	-62.60 ± 2.90
Hutch Calves	Oct 2018	49	6	45	-57.58 ± 2.90
	Jan 2019	25	48	27	-60.99 ± 2.90
	Mar 2019	25	48	27	-60.99 ± 2.90
	Jun 2019	25	48	27	-60.99 ± 2.90
	Sep 2019	25	48	27	-60.99 ± 2.90

[a]Estimated $\delta^{13}C_{CH4}$ using Chang et al. (2019) linear regression equation described in section 3.1.

The progression of manure from one component of the system to another also influenced the isotopic signature of CH_4 at the reference test site. Using a chamber to isolate sources of manure at different stages of the manure management on January 15th, 2020, we observed that a mixture of fresh volatile solids with urine on the floor of freestall barns yielded the most depleted $\delta^{13}C_{CH4}$ (-56.3 ± 0.4‰). Methane emitted from two separate manure piles at the solid drying area, however, had heavier $\delta^{13}C_{CH4}$ signatures (-39.1 ± 0.5‰ and -46.0 ± 0.9‰) (refer to Figure 1 for facility layout). The more depleted $\delta^{13}C_{CH4}$ observations were from a manure pile that was noticeably drier than the second sample. In comparison, measurements from manure lagoons using the mobile laboratory resulted in $\delta^{13}C_{CH4}$ of -43.4 ± 0.4‰.

3.2 Downwind Plume Sampling of Other Dairies in the Region

Isotopic signatures from CH_4 hotspots observed from downwind plume sampling of other dairies in the region were consistent with on-farm isotopic signatures (Table 4). For example, downwind plume sampling at Dairy I resulted in a depleted $\delta^{13}C_{CH4}$ value of -57.1 ± 3.4‰, representative of enteric CH_4, with an estimated $f_{enteric}$ of 0.75 ± 0.21 (Figure 5a-b, Table 4). At Dairy III, we observed isotopic signatures ranging from -59.9 ± 2.0‰ to -43.9 ± 0.7‰. The estimated $f_{enteric}$ and CH_4 flux footprint revealed that the most enriched isotopic signatures corresponded to CH_4 emissions from manure lagoons, while the most depleted isotopic signatures were from emissions from the corrals and manure lagoon areas (Figure 5, Table 4, Figures S1-S11). Within the same day, on June 25th, we observed two CH_4 hotspots with more enriched isotopic signatures, -44.5 ± 1.6‰ (Figure 5c-d) and -43.9 ± 0.7‰, which fall within the range of manure lagoon $\delta^{13}C_{CH4}$ observed at the reference test site, and a hotspot with a more depleted isotopic signature (-59.9 ± 2.0‰), similar to enteric fermentation sources observed at the reference test site. We observed a similar circumstance on March 24th—the flux footprint primarily captured the manure lagoon areas with a more enriched isotopic signature of -51.6 ± 1.2‰ in the early afternoon with predominantely southwesterly winds, but the flux footprints shifted to both corrals and lagoons in the late afternoon with predominantly northeasterly winds, resulting in a more depleted isotopic signature of -58.4 ± 2.9‰. The resulting $f_{enteric}$ of 0.41 ±

0.08 was estimated for the more enriched isotopic signature of -51.6 ± 1.2‰, meanwhile the more depleted isotopic signature of -58.4 ± 2.9‰ had a higher $f_{enteric}$ of 0.83 ± 0.19.

Isotopic signatures were also influenced by the distance between the location of measurements and dairy farm, as well as the proximity to other dairy farms. To illustrate this further, a CH_4 plume was observed approximately 140 m downwind of Dairy II, with a $\delta^{13}C_{CH4}$ value of -50.2 ± 1.5‰, a value that is representative of atmospheric mixing of CH_4 emissions from dairy manure lagoon and enteric fermentation sources. The largest contributing source to the CH_4 flux footprint was corrals and the corresponding $f_{enteric}$ was 0.32 ± 0.10, suggesting an additional source of CH_4 emissions with an enriched isotopic signature, such as manure piles in the corrals. We detected four CH_4 hotspots downwind of the Dairy Cluster with a narrow range of $\delta^{13}C_{CH4}$ values, -53.5 ± 2.3‰ to -50.4 ± 1.8‰. Different upwind areas of the dairy farms A-F were captured by the CH_4 flux footprint (Table 4, Figures S8-S11).

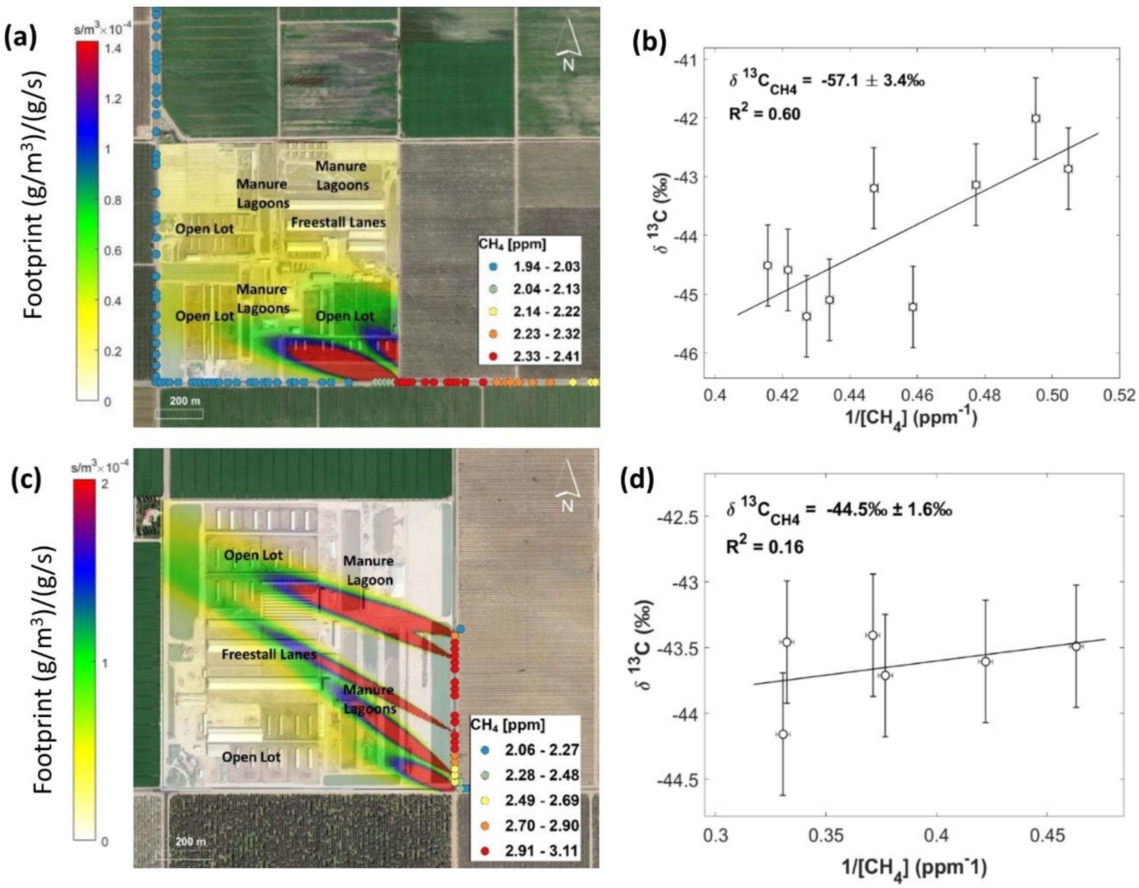

Figure 5. Examples of flux footprints from CH_4 hotspots downwind of other dairy farms. (a) Methane flux footprint of Dairy I on June 25th, 2019 using the mobile survey (colored points). The color gradient shows the relative contribution from the upwind areas where CH_4 was emitted. (b) Keeling plot using 15-second averages from the mobile survey shown in (a). (c) Methane flux footprint of Dairy III on June 25th, 2019 using the mobile survey. (d) Keeling plot using 15-second averages from the mobile survey shown in (c).

Table 4. Regional Isotopic Signatures of CH_4 Downwind from Dairy Farms.

Date[a]	**Start**	**End**	**Dairy**	**$\delta^{13}C_{CH4}$**	**R^2**	***p value***	**Predominant Wind Direction**	**Measurement Location Relative to Dairy Farm**	**Largest Contributing Sources to the Methane Flux Footprint**	**Fraction of Enteric Methane Emissions**[b]
6/25/2019	15:51:40	15:53:50	Dairy I	-57.1 ± 3.4	0.60	0.03	WNW	S	Corrals	0.75 ± 0.21
9/21/2018	18:05:01	18:09:30	Dairy II	-50.2 ± 1.5	0.18	0.01	W	E	Corrals	0.32 ± 0.10
3/24/2019	13:28:01	13:32:00	Dairy III	-51.6 ± 1.2	0.20	<.001	SW	E, S	Lagoons	0.41 ± 0.08
3/24/2019	17:53:01	17:55:13	Dairy III	-58.4 ± 2.9	0.33	0.01	NE	S	Corrals & Lagoons	0.83 ± 0.19
6/25/2019	14:02:00	14:05:30	Dairy III	-59.9 ± 2.0	0.23	<.001	NW	E, S, W	Corrals & Lagoons	0.93 ± 0.13
6/25/2019	15:17:00	15:18:28	Dairy III	-44.5 ± 1.6	0.16	0.62	WNW	E	Lagoons	-0.04 ± 0.10
6/25/2019	17:11:30	17:15:00	Dairy III	-43.9 ± 0.7	0.02	0.22	NW	S, E	Lagoons	-0.08 ± 0.05
9/21/2018	17:18:12	17:23:36	Dairy Cluster	-52.9 ± 1.6	0.13	<.001	WNW	In-between	Dairies D-F	0.49 ± 0.10
3/24/2019	14:16:59	14:23:34	Dairy Cluster	-53.5 ± 2.3	0.06	<.001	NNW	In-between	Dairies A-F	0.53 ± 0.15
6/24/2019	16:06:41	16:12:05	Dairy Cluster	-50.4 ± 1.8	0.02	0.06	NW	In-between	Dairies D-F	0.33 ± 0.12
6/25/2019	14:14:54	14:20:28	Dairy Cluster	-52.6 ± 2.6	0.05	0.04	WNW	In-between	Dairies C-F	0.47 ± 0.17

[a] Date format: M/DD/YYYY.
[b] Standard errors are reported for $\delta^{13}C_{CH4}$ isotopic signatures.

4 Discussion and Conclusion

Stable carbon isotope measurements of CH_4 can be a valuable source apportionment technique to distinguish between enteric and manure CH_4. At the reference test site farm, we found a clear separation of $\delta^{13}C_{CH4}$ signatures between enteric fermentation source areas (more depleted: -69.7 ± 0.6‰ to -51.6 ± 0.1‰) and manure lagoons (more enriched: -49.5 ± 0.05‰ to -40.5 ± 0.2‰). These source signatures were relatively invariant across season, particularly from manure lagoons, and were always different from one another by at least ~8‰. Additionally, isotopic signatures from CH_4 hotspots observed from remote mobile surveys were consistent with on-farm isotopic signatures. Measurements of ^{13}C of CH_4 downwind of dairy farms may be a useful tool to monitor and quantify enteric:manure ratios with changes in mitigation (Marklein et al., 2020). As shown in this study, isotopic signatures of CH_4 downwind of dairy farms can be used to estimate the fraction of contributing sources, such as from manure lagoons and enteric fermentation source areas. Most CH_4 mitigation strategies address CH_4 emitted from enteric fermentation, such as through feed additives (Honan et al., 2021), or manure emissions by changing management techniques (Joshi, 2020). As governing bodies undertake mitigation strategies to reduce CH_4 emissions from enteric fermentation or dairy manure management, it is essential to verify mitigation effectiveness. In California, for example, numerous dairy farms have recently adopted or plan to install digesters in the near future to capture and convert CH_4 from manure lagoons into fuel. An important area of future research is to quantify the effect of mitigation strategies by comparing $\delta^{13}C_{CH4}$ downwind of dairy farms before and after installation of digesters.

Isotopic signatures in this study agree with previous research showing that manure CH_4 is more enriched in ^{13}C than enteric CH_4. Our on-farm measurements, however, show that manure lagoon CH_4 is relatively more enriched in ^{13}C than previously reported in Southern California. Townsend-Small et al. (2012) reported a $^{13}C_{CH4}$ range of -52.4‰ to -50.3‰ from manure biofuel from a manure digester facility and Viatte et al. (2017) reported ^{13}C of CH_4 of about -57‰ near manure lagoons. This may be explained by differences in CH_4 generation processes and manure management differences between Southern California and San Joaquin Valley. Dairies in the San Joaquin Valley predominately use flush systems and store manure in lagoons, while Southern California dairies typically operate dry lots that forgo flushing manure from the feedlanes (Meyer et al., 2019; Marklein et al., 2020). Nevertheless, all California farms produce liquid manure from flushing solids in the milking parlor (Meyer et al., 2019). Although Viatte et al. (2017) reported a more depleted ^{13}C of CH_4 of about -57‰ near manure lagoons compared to this study, they also observed an ~8‰ fractionation between enteric CH_4 and manure CH_4, consistent with our findings of isotopic fractionation between manure lagoons and enteric CH_4 from freestall barns. There may also be differences in the stable carbon isotope composition of feed and differences in biogeochemical factors that play a key role in determining which microbial communities and pathways promote or inhibit CH_4 generation from dairy manure management, and in turn affect the isotopic signature of CH_4 emissions. These include pH, dissolved oxygen level, temperature, volatile fatty acids, chemical composition of the substrate, total nitrogen, and nutrient composition (Amon et al., 2007; Weiland, 2010).

Future work is needed to explain the isotopic composition of CH_4 emissions from manure lagoons. This area of research can provide important information on the dominant microbial communities and biogeochemical processes, which can inform mitigation efforts to reduce CH_4 emissions from the dairy sector. In our study, whole air sample analysis using IRMS (Table 1) showed that CH_4 emissions from cell 1 were relatively more enriched in $\delta^{13}C$ (-42.91 ± 0.23‰)

and more depleted in the hydrogen isotopic composition of CH_4 (δ^2H-CH_4 or δD-CH_4, -326 ± 4‰) than CH_4 from the primary lagoon ($\delta^{13}C$-CH_4 = -50.13 ± 0.23‰, δ^2H-CH_4 = -263 ± 4‰). The differences in the isotopic signatures of these samples indicate that CH_4 generated from cell 1 may be explained primarily by acetate fermentation, but CH_4 generated from the primary lagoon may have undergone further processes such as partial oxidation or CO_2 reduction. Substrate depletion may also explain this variation, but additional measurements of $\delta^{13}C$ of volatile solids or CO_2 concentrations would be needed to confirm isotopically fractionated substrates. During acetate fermentation, CH_4 and CO_2 are commonly formed simultaneously. Reduction of CO_2 may further transform the generated CO_2 into CH_4. In the influential study conducted by Whiticar et al. (1986), CH_4 generated from pure acetate fermentation resulted in $\delta^{13}C$-CH_4 ranging from -60 to -33‰, whereas CH_4 from pure CO_2 reduction had $\delta^{13}C$-CH_4 values ranging from -110 to -60‰. However, bacterial oxidation in the substrate may affect these pathways before being emitted to the atmosphere, and consequently enrich ^{13}C values of CH_4. Measurements of δ^2H-CH_4 can provide information about partial oxidation since this process enriches $\delta^{13}C$-CH_4 and δ^2H-CH_4 values (Coleman et al., 1981). A future study examining $\delta^{13}C$ and δ^2H of methane and $\delta^{13}C$-CO_2 from dairy manure lagoon waste is necessary to confirm the dominant processes contributing to the enriched $\delta^{13}C_{CH4}$ signatures from California dairy manure lagoons.

Isotopic signatures of CH_4 from enteric fermentation depend on the C isotopic ratio of foods, specifically with the proportion of plants with C3 and C4 photosynthetic pathways in cattle diets (Metges et al., 1990; Levin et al., 1993; Schulze et al., 1998; Bilek et al., 2001). A diet consisting mostly of C3 plants (e.g., wheat) has been shown to generate more depleted $\delta^{13}C_{CH4}$ than a diet of C4 plants (e.g., corn) (Levin et al., 1993; Schwietzke et al., 2016). A database of studies found that ruminants fed a diet of more than 60% C4 plants emit CH_4 with $\delta^{13}C_{CH4}$ signatures of -54.6 ± 3.1‰, whereas ruminants fed a C3 diet emit CH_4 with $\delta^{13}C_{CH4}$ signatures of -69.4 ± 3.1‰ (Schwietzke et al., 2016). This ~15‰ difference is about the same difference between ^{13}C of C3 and C4 feeds. Furthermore, there is a ~41‰ difference between feed and CH_4 regardless of ruminant species and diet (Schaefer & Whiticar, 2008). Future studies could explore the relationship between diet and CH_4 isotope composition across seasons from different cattle production groups. To improve source apportionment of regional CH_4 emissions in top-down studies, it is important to consider direct measurements of $\delta^{13}C_{CH4}$ of enteric methane given that it varies depending on diet composition.

We have shown that $\delta^{13}C$ measurements of atmospheric CH_4 using a mobile platform can be used for source attribution of enteric and manure methane. Our findings show that CH_4 from manure lagoons is more enriched in $\delta^{13}C$ than CH_4 from enteric fermentation across seasons on average by 14 ± 2‰. This has implications to track the effectiveness of mitigation strategies by measuring $\delta^{13}C_{CH4}$ to quantify enteric: manure ratios over time. In addition, this study contributes to a body of knowledge dedicated to investigating the sources and processes responsible for the increasing global mole fraction of atmospheric methane. Future work could explore whether $\delta^{13}C_{CH4}$ signatures change with mitigation efforts. Additional measurements using $\delta^{13}C$ and $\delta^{2}H$ of CH_4 and $\delta^{13}C\text{-}CO_2$ could elucidate which methane generation processes drive manure lagoon emissions. Major differences in $\delta^{13}C_{CH4}$ from dairy farms among regions underscore the importance of $\delta^{13}C_{CH4}$ measurements at local scales for global analyses.

Acknowledgments

We thank our dairy collaborator for site access and collaboration. This work was supported by the University of California, Office of the President, Laboratory Fee Research Program (grant

LFR-18-548581). V. Carranza also acknowledges funding from the National Science Foundation Graduate Research Fellowship Program and the University of California, Riverside Environmental Dynamics and GeoEcology (EDGE) Institute. Work at Lawrence Berkeley National Laboratory was also supported by Contractor Supporting Research (*CSR*) under Contract No.DE-AC02-05CH11231. The authors' views and opinions expressed herein do not necessarily state or reflect those of the United States Government or any agency thereof, or The Regents of the University of California. We thank Michael Rodriguez, Casaundra Caruso, Yifan Ding, Sajjan Heerah, Celia Limon, Alison Marklein, and Cindy Yañez for help with field work.

Open Research

The dataset for this paper is available online at the Dryad Digital Repository: https://doi.org/10.6086/D1W10G.

References

Amon, T., Amon, B., Kryvoruchko, V., Zollitsch, W., Mayer, K., & Gruber, L. (2007). Biogas production from maize and dairy cattle manure-Influence of biomass composition on the methane yield. *Agriculture, Ecosystems and Environment*, *118*(1–4), 173–182. https://doi.org/10.1016/j.agee.2006.05.007

Bilek, R. S., Tyler, S. C., Kurihara, M., & Yagi, K. (2001). Investigation of cattle methane production and emission over a 24-hour period using measurements of $\delta^{13}C$ and δD of emitted CH_4 and rumen water. *Journal of Geophysical Research: Atmospheres*, *106*(D14), 15405–15413. https://doi.org/10.1029/2001JD900177

Blake, D. R., Smith, T. W., Chen, T.-Y., Whipple, W. J., & Rowland, F. S. (1994). Effects of biomass burning on summertime nonmethane hydrocarbon concentrations in the Canadian wetlands. *Journal of Geophysical Research*, *99*(D1), 1699. https://doi.org/10.1029/93jd02598

Chang, J., Peng, S., Ciais, P., Saunois, M., Dangal, S. R. S., Herrero, M., Havlík, P., Tian, H., & Bousquet, P. (2019). Revisiting enteric methane emissions from domestic ruminants and their δ13CCH4 source signature. *Nature Communications*, *10*(1). https://doi.org/10.1038/s41467-019-11066-3

Coleman, D., Risatti, J., & Schoell, M. (1981). Fractionation of carbon and hydrogen isotopes by methane-oxidizing bacteria. *Geochimica et Cosmochimica*, *45*, 1033–1037. https://www.sciencedirect.com/science/article/pii/0016703781901290

Colman, J. J., Swanson, A. L., Meinardi, S., Sive, B. C., Blake, D. R., & Rowland, F. S. (2001).

Description of the analysis of a wide range of volatile organic compounds in whole air samples collected during PEM-Tropics A and B. *Analytical Chemistry*, *73*(15), 3723–3731. https://doi.org/10.1021/ac010027g

Cui, Y. Y., Brioude, J., Angevine, W. M., Peischl, J., McKeen, S. A., Kim, S. W., Andrew Neuman, J., Henze, D. K., Bousserez, N., Fischer, M. L., Jeong, S., Michelsen, H. A., Bambha, R. P., Liu, Z., Santoni, G. W., Daube, B. C., Kort, E. A., Frost, G. J., Ryerson, T. B., … Trainer, M. (2017). Top-down estimate of methane emissions in California using a mesoscale inverse modeling technique: The San Joaquin Valley. *Journal of Geophysical Research*, *122*(6), 3686–3699. https://doi.org/10.1002/2016JD026398

Dlugokencky, E. J., Masarie, K. A., Lang, P. M., & Tans, P. P. (1998). Continuing decline in the growth rate of the atmospheric methane burden. *Nature*, *393*(6684), 447–450. https://doi.org/https://doi.org/10.1038/30934

Dlugokencky, E. J., Nisbet, E. G., Fisher, R., & Lowry, D. (2011). Global atmospheric methane: budget, changes and dangers. *Philosophical Transactions of the Royal Society A: Mathematical, Physical and Engineering Sciences*, *369*(1943), 2058–2072. https://doi.org/10.1098/rsta.2010.0341

Duren, R. M., Thorpe, A. K., Foster, K. T., Rafiq, T., Hopkins, F. M., Yadav, V., Bue, B. D., Thompson, D. R., Conley, S., Colombi, N. K., Frankenberg, C., McCubbin, I. B., Eastwood, M. L., Falk, M., Herner, J. D., Croes, B. E., Green, R. O., & Miller, C. E. (2019). California's methane super-emitters. *Nature*, *575*(7781), 180–184. https://doi.org/10.1038/s41586-019-1720-3

Fry, B. (2006). *Stable isotope ecology*. Springer.

Hoheisel, A., Yeman, C., Dinger, F., Eckhardt, H., & Schmidt, M. (2019). An improved method for mobile characterisation of δ 13 CH 4 source signatures and its application in Germany. *Atmospheric Measurement Techniques*, *12*(2), 1123–1139. https://doi.org/10.5194/amt-12-1123-2019

Honan, M., Feng, X., Tricarico, J. M., & Kebreab, E. (2021). Feed additives as a strategic approach to reduce enteric methane production in cattle: Modes of action, effectiveness and safety. *Animal Production Science*. https://doi.org/10.1071/AN20295

Hopkins, F. M., Ehleringer, J. R., Bush, S. E., Duren, R. M., Miller, C. E., Lai, C. T., Hsu, Y. K., Carranza, V., & Randerson, J. T. (2016). Mitigation of methane emissions in cities: How new measurements and partnerships can contribute to emissions reduction strategies. *Earth's Future*, *4*(9), 408–425. https://doi.org/10.1002/2016EF000381

Hopkins, F. M., Kort, E. A., Bush, S. E., Ehleringer, J. R., Lai, C. T., Blake, D. R., & Randerson, J. T. (2016). Spatial patterns and source attribution of urban methane in the los angeles basin. *Journal of Geophysical Research*, *121*(5), 2490–2507. https://doi.org/10.1002/2015JD024429

Jeong, S., Hsu, Y. K., Andrews, A. E., Bianco, L., Vaca, P., Wilczak, J. M., & Fischer, M. L. (2013). A multitower measurement network estimate of California's methane emissions. *Journal of Geophysical Research Atmospheres*, *118*(19), 11,339-11,351. https://doi.org/10.1002/jgrd.50854

Jeong, S., Newman, S., Zhang, J., Andrews, A. E., Bianco, L., Bagley, J., Cui, X., Graven, H., Kim, J., Salameh, P., LaFranchi, B. W., Priest, C., Campos-Pineda, M., Novakovskaia, E., Sloop, C. D., Michelsen, H. A., Bambha, R. P., Weiss, R. F., Keeling, R., & Fischer, M. L. (2016). Estimating methane emissions in California's urban and rural regions using multitower observations. *Journal of Geophysical Research: Atmospheres*, *121*(21), 13,031-13,049. https://doi.org/10.1002/2016JD025404

Joshi, G. (2020, January). Less methane by 2030. *Journal of Nutrient Management*, 18–19. https://jofnm.com/article-37-Less-methane-by-2030.html

Keeling, C. D. (1958). The concentration and isotopic abundances of atmospheric carbon dioxide in rural areas. *Geochimica et Cosmochimica Acta*, *13*, 322–334. https://doi.org/https://doi.org/10.1016/0016-7037(58)90033-4

Levin, I., Bergamaschi, P., Dörr, H., & Trapp, D. (1993). Stable isotopic signature of methane from major sources in Germany. *Chemosphere*, *26*(1–4), 161–177. https://doi.org/10.1016/0045-6535(93)90419-6

Litvak, E., Bijoor, N. S., & Pataki, D. E. (2014). Adding trees to irrigated turfgrass lawns may be a water-saving measure in semi-arid environments. *Ecohydrology*, *7*(5), 1314–1330. https://doi.org/10.1002/eco.1458

Lowry, D., Fisher, R. E., France, J. L., Coleman, M., Lanoisellé, M., Zazzeri, G., Nisbet, E. G., Shaw, J. T., Allen, G., Pitt, J., & Ward, R. S. (2020). Environmental baseline monitoring for shale gas development in the UK: Identification and geochemical characterisation of local source emissions of methane to atmosphere. *Science of the Total Environment*, *708*, 134600. https://doi.org/10.1016/j.scitotenv.2019.134600

Marklein, A. R., Meyer, D., Fischer, M. L., Jeong, S., Rafiq, T., Carr, M., & Hopkins, F. M. (2020). Facility scale inventory of dairy methane emissions in California: Implications for mitigation. *Earth System Science Data*, *August*. https://doi.org/https://doi.org/10.5194/essd-2020-133

Metges, C., Kempe, K., & Schmidt, H.-L. (1990). Dependence of the carbon-isotope contents of breath carbon dioxide, milk, serum and rumen fermentation products on the δ13C value of food in dairy cows. *British Journal of Nutrition*, *63*(2), 187–196. https://doi.org/10.1079/bjn19900106

Meyer, D., Heguy, J., Karle, B., & Robinson, P. (2019). *Characterize Physical and Chemical Properties of Manure in California Dairy Systems to Improve Greenhouse Gas Emission Estimates. Final Report: Contract No. 16RD002.* (pp. 1–70). California Air Resources Board and the California Environmental Protection Agency.

Miles, N. L., Martins, D. K., Richardson, S. J., Rella, C. W., Arata, C., Lauvaux, T., Davis, K. J., Barkley, Z. R., McKain, K., & Sweeney, C. (2018). Calibration and field testing of cavity ring-down laser spectrometers measuring CH4, CO2, and δ13CH4 deployed on towers in the Marcellus Shale region. *Atmospheric Measurement Techniques*, *11*(3), 1273–1295. https://doi.org/10.5194/amt-11-1273-2018

Miller, D. J., Sun, K., Tao, L., Pan, D., Zondlo, M. A., Nowak, J. B., Liu, Z., Diskin, G., Sachse, G., Beyersdorf, A., Ferrare, R., & Scarino, A. J. (2015). Ammonia and methane dairy emission plumes in the San Joaquin valley of California from individual feedlot to regional scales. *Journal of Geophysical Research*, *120*(18), 9718–9738. https://doi.org/10.1002/2015JD023241

Miller, S. M., Wofsy, S. C., Michalak, A. M., Kort, E. A., Andrews, A. E., Biraud, S. C., Dlugokencky, E. J., Eluszkiewicz, J., Fischer, M. L., Janssens-Maenhout, G., Miller, B. R., Miller, J. B., Montzka, S. A., Nehrkorn, T., & Sweeney, C. (2013). Anthropogenic emissions of methane in the United States. *Proceedings of the National Academy of Sciences of the United States of America*, *110*(50), 20018–20022. https://doi.org/10.1073/pnas.1314392110

Mullinax, D., Meyer, D., & Summer, D. (2020). *Small Dairy Climate Change Research: An economic evaluation of strategies for methane emission reduction effectiveness and appropriateness in small and large California dairies*. https://www.cdfa.ca.gov/oefi/research/docs/CDFA_SmallDairyResearch_Final_Report.pdf

Naus, S., Montzka, S. A., Pandey, S., Basu, S., Dlugokencky, E. J., & Krol, M. (2019). Constraints and biases in a tropospheric two-box model of OH. *Atmospheric Chemistry and Physics*, *19*(1), 407–424. https://doi.org/10.5194/acp-19-407-2019

Nisbet, E. G., Dlugokencky, E. J., & Bousquet, P. (2014). Methane on the Rise—Again. *Science*, *343*(6170), 493–495. https://doi.org/10.1017/CBO9781107415324.004

Nisbet, E. G., Dlugokencky, E. J., Manning, M. R., Lowry, D., Fisher, R. E., France, J. L., Michel, S. E., Miller, J. B., White, J. W. C., Vaughn, B., Bousquet, P., Pyle, J. A., Warwick, N. J., Cain, M., Brownlow, R., Zazzeri, G., Lanoiselle, M., Manning, A. C., Gloor, E., … Ganesan, A. L. (2016). Rising atmospheric methane: 2007–2014 growth and isotopic shift. *Global Biogeochemical Cycles*, *30*, 1475–1492. https://doi.org/10.1002/2015GB005323

Nisbet, E. G., Manning, M. R., Dlugokencky, E. J., Fisher, R. E., Lowry, D., Michel, S. E., Myhre, C. L., Platt, S. M., Allen, G., Bousquet, P., Brownlow, R., Cain, M., France, J. L., Hermansen, O., Hossaini, R., Jones, A. E., Levin, I., Manning, A. C., Myhre, G., … White, J. W. C. (2019). Very Strong Atmospheric Methane Growth in the 4 Years 2014–2017: Implications for the Paris Agreement. *Global Biogeochemical Cycles*, *33*(3), 318–342. https://doi.org/10.1029/2018GB006009

Owen, J. J., & Silver, W. L. (2015). Greenhouse gas emissions from dairy manure management: a review of field-based studies. *Global Change Biology*, *21*(2), 550–565. https://doi.org/10.1111/gcb.12687

Pataki, D. E., Ehleringer, J. R., Flanagan, L. B., Yakir, D., Bowling, D. R., Still, C. J., Buchmann, N., Kaplan, J. O., & Berry, J. A. (2003). The application and interpretation of Keeling plots in terrestrial carbon cycle research. *Global Biogeochemical Cycles*, *17*(1), 1022. https://doi.org/10.1029/2001GB001850

Rigby, M., Montzka, S. A., Prinn, R. G., C White, J. W., Young, D., Lunt, M. F., Ganesan, A. L., Manning, A. J., Simmonds, P. G., Salameh, P. K., Harth, C. M., Weiss, R. F., Fraser, P. J., Paul Steele, L., Krummel, P. B., McCulloch, A., & Park, S. (2017). Role of atmospheric oxidation in recent methane growth. *Proceedings of the National Academy of Sciences*, *114*(21), 5373–5377. https://doi.org/10.1073/pnas.1616426114

Schaefer, H., Fletcher, S. E. M., Veidt, C., Lassey, K. R., Brailsford, G. W., Bromley, T. M., Dlugokencky, E. J., Michel, S. E., Miller, J. B., Levin, I., Lowe, D. C., Martin, R. J., Vaughn, B. H., & White, J. W. C. (2016). A 21st-century shift from fossil-fuel to biogenic methane emissions indicated by 13CH4. *Science*, *352*(6281), 80–84. https://doi.org/10.1126/science.aad2705

Schaefer, H., & Whiticar, M. J. (2008). Potential glacial-interglacial changes in stable carbon isotope ratios of methane sources and sink fractionation. *Global Biogeochemical Cycles*, *22*(1). https://doi.org/10.1029/2006GB002889

Schulze, E., Lohmeyer, S., & Giese, W. (1998). Determination of13C/12C-ratios in rumen produced methane and CO2 of cows, sheep and camels. *Isotopes in Environmental and Health Studies*, *34*(1–2), 75–79. https://doi.org/10.1080/10256019708036334

Schwietzke, S., Sherwood, O. A., Bruhwiler, L. M. P., Miller, J. B., Etiope, G., Dlugokencky, E. J., Michel, S. E., Arling, V. A., Vaughn, B. H., White, J. W. C., & Tans, P. P. (2016). Upward revision of global fossil fuel methane emissions based on isotope database. *Nature*, *538*(7623), 88–91. https://doi.org/10.1038/nature19797

Thirumalai, K., Singh, A., & Ramesh, R. (2011). A MATLAB^{TM} code to perform weighted linear regression with (correlated or uncorrelated) errors in bivariate data. *Journal of the Geological Society of India*, *77*(4), 377–380. https://doi.org/10.1007/s12594-011-0044-1

Thiruvenkatachari, R., Carranza, V., Ahangar, F., Marklein, A., Hopkins, F., & Venkatram, A. (2020). Uncertainty in using dispersion models to estimate methane emissions from manure lagoons in dairies. *Agricultural and Forest Meteorology*. https://doi.org/10.1016/j.agrformet.2020.108011

Townsend-Small, A., Tyler, S. C., Pataki, D. E., Xu, X., & Christensen, L. E. (2012). Isotopic measurements of atmospheric methane in Los Angeles, California, USA: Influence of "fugitive" fossil fuel emissions. *Journal of Geophysical Research: Atmospheres*, *117*(D7), n/a-n/a. https://doi.org/10.1029/2011JD016826

Trousdell, J. F., Conley, S. A., Post, A., & Faloona, I. C. (2016). Observing entrainment mixing, photochemical ozone production, and regional methane emissions by aircraft using a simple mixed-layer framework. *Atmospheric Chemistry and Physics*, *16*(24), 15433–15450. https://doi.org/10.5194/acp-16-15433-2016

Turner, A. J., Frankenberg, C., Wennberg, P. O., & Jacob, D. J. (2017). Ambiguity in the causes for decadal trends in atmospheric methane and hydroxyl. *Proceedings of the National Academy of Sciences*, *114*(21), 5367–5372. https://doi.org/10.1073/pnas.1616020114

United Nations Environment Programme and Climate and Clean Air Coalition. (2021). *Global Methane Assessment: Benefits and Costs of Mitigating Methane Emissions. Nairobi: United Nations Environment Programme*. https://doi.org/978-92-807-3854-4

Viatte, C., Lauvaux, T., Hedelius, J. K., Parker, H., Chen, J., Jones, T., Franklin, J. E., Deng, A. J., Gaudet, B., Verhulst, K., Duren, R., Wunch, D., Roehl, C., Dubey, M. K., Wofsy, S., & Wennberg, P. O. (2017a). Methane emissions from dairies in the Los Angeles Basin. *Atmospheric Chemistry and Physics*, *17*(12), 7509–7528. https://doi.org/10.5194/acp-17-7509-2017

Viatte, C., Lauvaux, T., Hedelius, J. K., Parker, H., Chen, J., Jones, T., Franklin, J. E., Deng, A. J., Gaudet, B., Verhulst, K., Duren, R., Wunch, D., Roehl, C., Dubey, M. K., Wofsy, S., & Wennberg, P. O. (2017b). Methane emissions from dairies in the Los Angeles Basin. *Atmospheric Chemistry and Physics*, *17*(12), 7509–7528. https://doi.org/10.5194/acp-17-7509-2017

Wecht, K. J., Jacob, D. J., Sulprizio, M. P., Santoni, G. W., Wofsy, S. C., Parker, R., Bösch, H., & Worden, J. (2014). Spatially resolving methane emissions in California: constraints from the CalNex aircraft campaign and from present (GOSAT, TES) and future (TROPOMI, geostationary) satellite observations. *Atmospheric Chemistry and Physics*, *14*(15), 8173–8184. https://doi.org/10.5194/acp-14-8173-2014

Weiland, P. (2010). Biogas production: Current state and perspectives. *Applied Microbiology and Biotechnology*, *85*(4), 849–860. https://doi.org/10.1007/s00253-009-2246-7

Whiticar, M., Faber, E., Acta, M. S.-G. et C., & 1986, U. (1986). Biogenic methane formation in marine and freshwater environments: CO2 reduction vs. acetate fermentation—isotope evidence. *Geochimica et Cosmochimica Acta*, *50*(5), 693–709. https://doi.org/https://doi.org/10.1016/0016-7037(86)90346-7

Worden, J. R., Bloom, A. A., Pandey, S., Jiang, Z., Worden, H. M., Walker, T. W., Houweling, S., & Röckmann, T. (2017). Reduced biomass burning emissions reconcile conflicting estimates of the post-2006 atmospheric methane budget. *Nature Communications*, *8*(1), 1–11. https://doi.org/10.1038/s41467-017-02246-0

Yarnes, C. (2013). δ13C and δ2H measurement of methane from ecological and geological sources by gas chromatography/combustion/pyrolysis isotope-ratio mass spectrometry. *Rapid Communications in Mass Spectrometry*, *27*(9), 1036–1044. https://doi.org/10.1002/rcm.6549

York, D., Evensen, N. M., Martínez, M. L., & De Basabe Delgado, J. (2004). Unified equations for the slope, intercept, and standard errors of the best straight line. *American Journal of Physics*, *72*(3), 367–375. https://doi.org/10.1119/1.1632486

Journal of Geophysical Research: Biogeosciences

Supporting Information for

Isotopic Signatures of Methane Emissions from Dairy Farms in California's San Joaquin Valley

Valerie Carranza[1], Brenna Biggs[2], Deanne Meyer[3], Amy Townsend-Small[4], Ranga Rajan Thiruvenkatachari[5], Akula Venkatram[5], Marc L. Fischer[6], Francesca M. Hopkins[1]

[1]Department of Environmental Sciences & Environmental Dynamics and GeoEcology (EDGE) Institute, University of California, Riverside, CA 92521
[2]Department of Chemistry, University of California, Irvine, Irvine, CA 92697
[3]Department of Animal Science, University of California, Davis, Davis, CA 95616
[4]Departments of Geology and Geography, University of Cincinnati, Cincinnati, OH 45221
[5]Department of Mechanical Engineering, University of California, Riverside, CA 92521, USA
[6] Energy Technology Area, Lawrence Berkeley National Laboratory, Berkeley, California, USA

Contents of this file

Introduction

The Supporting Information includes additional information about the isotopic signatures downwind of dairy farms (Table 4). It includes time series plots of the CH_4 hotspot, Keeling plots, location of the CH_4 measurements, wind direction, and CH_4 flux footprints of the CH_4 hotspots estimated by the Eulerian numerical dispersion model. The data is averaged to 15 sec intervals.

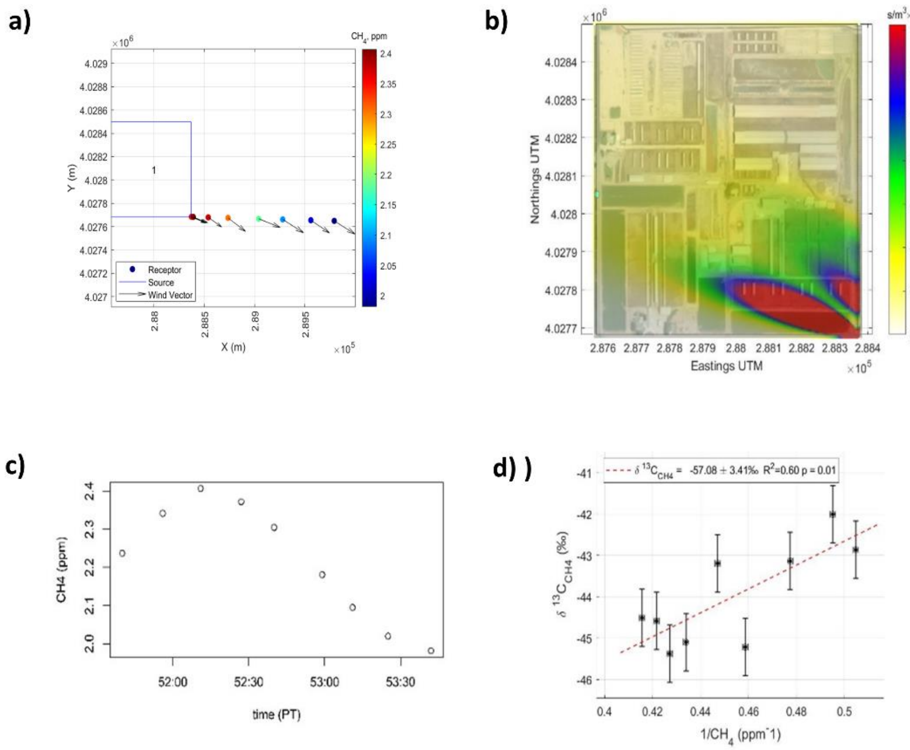

Figure S1. Isotopic signatures downwind of Dairy I on June 25th, 2019 from 15:51:40-15:53:50. a) Mobile platform measurements of 15-sec averaged CH_4 mole fractions (Receptor) downwind of Dairy I (Source). b) Methane flux footprint of Dairy I using the mobile survey shown in (a). The color gradient shows the relative contribution from the upwind areas where CH_4 was emitted. (c) Time series plot using 15-second averages from the mobile survey shown in (a). (d) Keeling plot using 15-second averages from the mobile survey shown in (a).

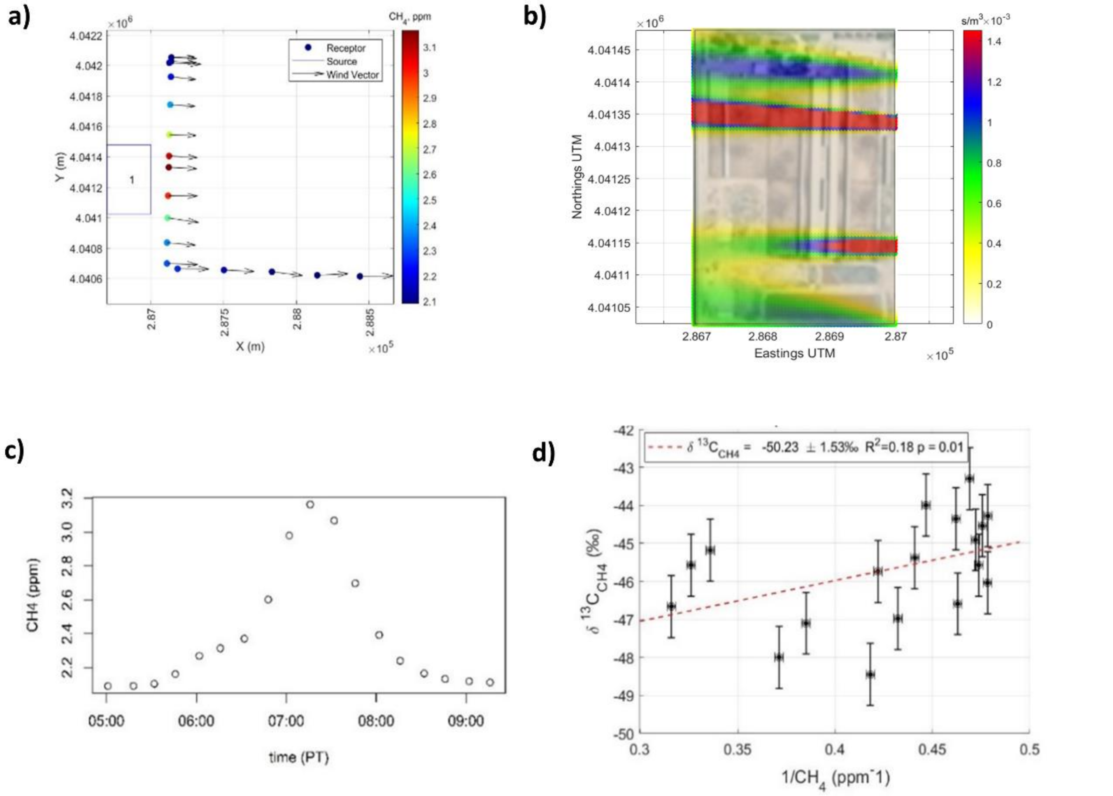

Figure S2. Isotopic signatures downwind of Dairy II on September 21st, 2018 from 18:05:01-18:09:30. a) Mobile platform measurements of 15-sec averaged CH_4 mole fractions (Receptor) downwind of Dairy II (Source). b) Methane flux footprint of Dairy II using the mobile survey shown in (a). The color gradient shows the relative contribution from the upwind areas where CH_4 was emitted. (c) Time series plot using 15-second averages from the mobile survey shown in (a). (d) Keeling plot using 15-second averages from the mobile survey shown in (a).

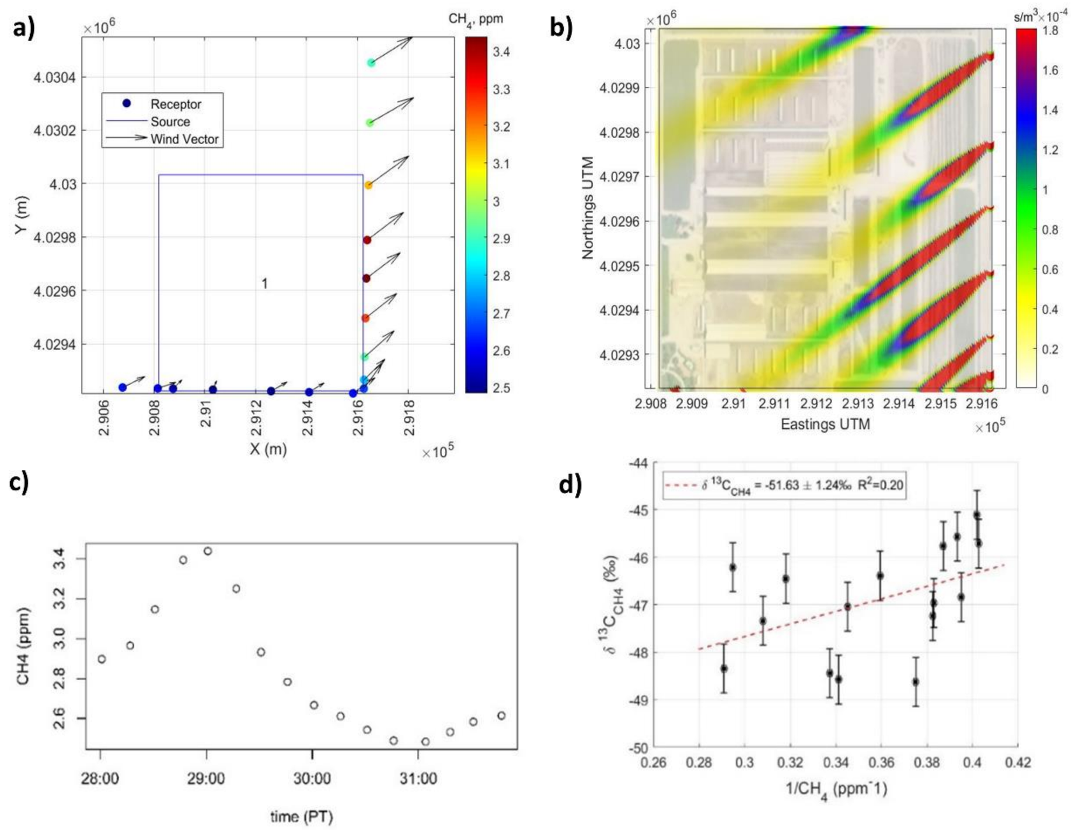

Figure S3. Isotopic signatures downwind of Dairy III on March 24th, 2019 from 13:28:01-13:32:00. a) Mobile platform measurements of 15-sec averaged CH_4 mole fractions (Receptor) downwind of Dairy III (Source). b) Methane flux footprint of Dairy III using the mobile survey shown in (a). The color gradient shows the relative contribution from the upwind areas where CH_4 was emitted. (c) Time series plot using 15-second averages from the mobile survey shown in (a). (d) Keeling plot using 15-second averages from the mobile survey shown in (a).

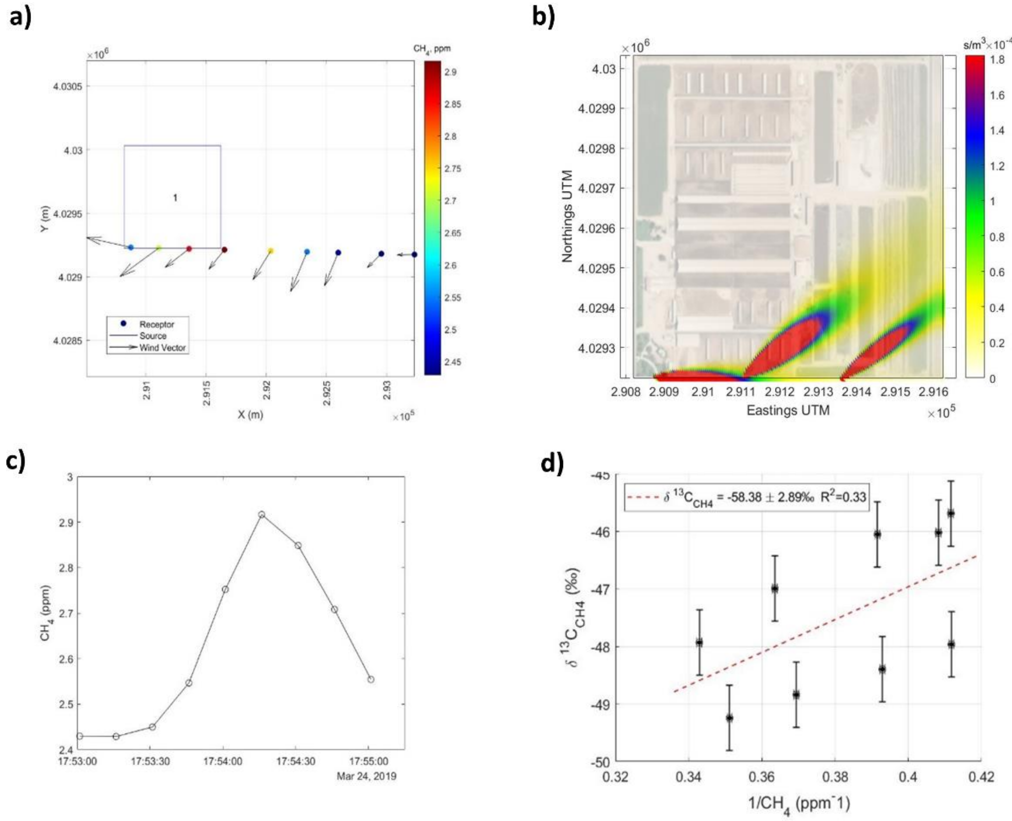

Figure S4. Isotopic signatures downwind of Dairy III on March 24th, 2019 from 17:53:01-17:55:13. a) Mobile platform measurements of 15-sec averaged CH_4 mole fractions (Receptor) downwind of Dairy III (Source). b) Methane flux footprint of Dairy III using the mobile survey shown in (a). The color gradient shows the relative contribution from the upwind areas where CH_4 was emitted. (c) Time series plot using 15-second averages from the mobile survey shown in (a). (d) Keeling plot using 15-second averages from the mobile survey shown in (a).

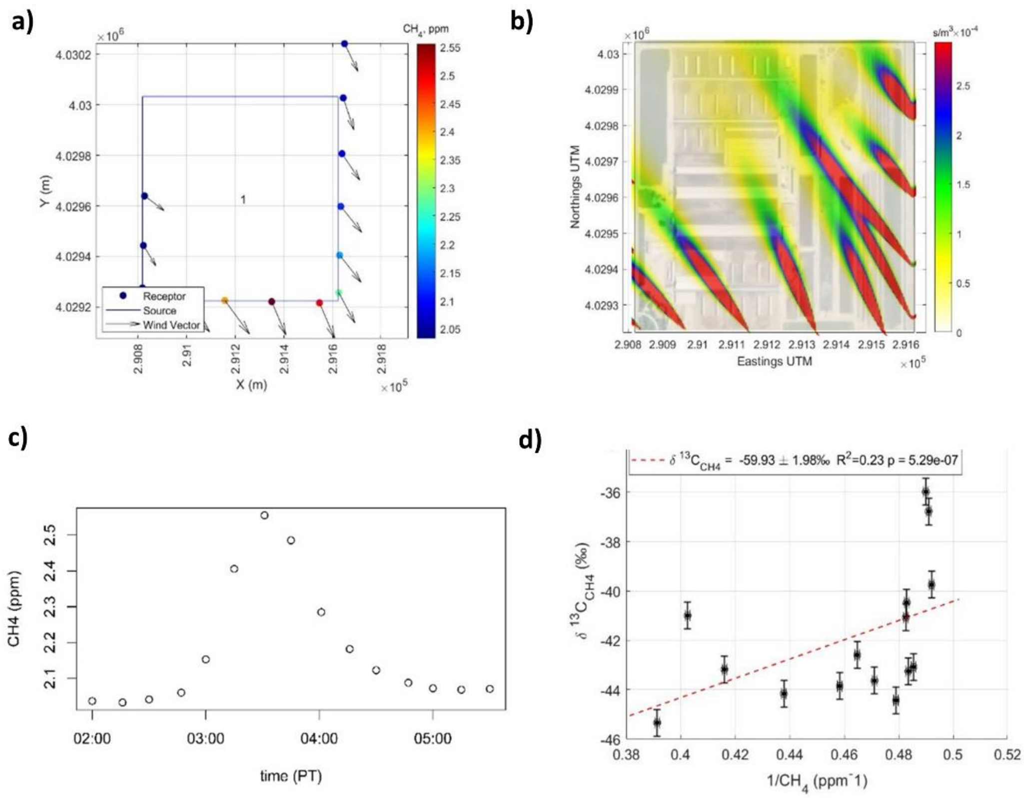

Figure S5. Isotopic signatures downwind of Dairy III on June 25th, 2019 from 14:02:00-14:05:30. a) Mobile platform measurements of 15-sec averaged CH_4 mole fractions (Receptor) downwind of Dairy III (Source). b) Methane flux footprint of Dairy III using the mobile survey shown in (a). The color gradient shows the relative contribution from the upwind areas where CH_4 was emitted. (c) Time series plot using 15-second averages from the mobile survey shown in (a). (d) Keeling plot using 15-second averages from the mobile survey shown in (a).

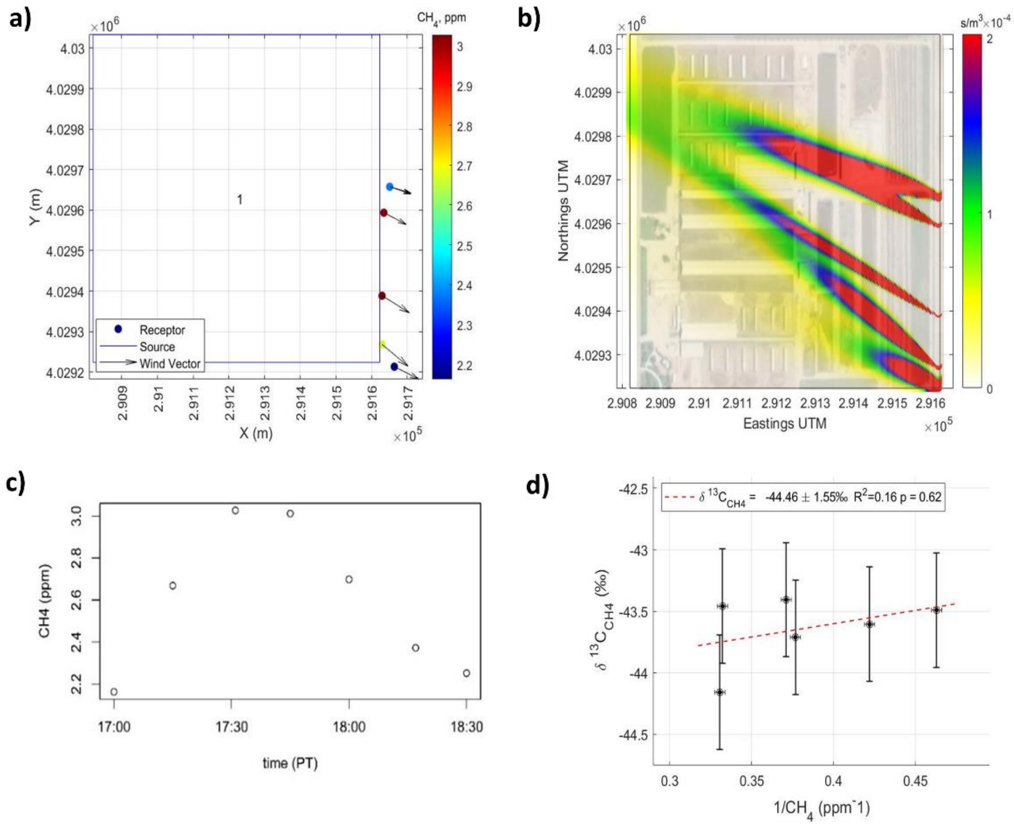

Figure S6. Isotopic signatures downwind of Dairy III on June 25th, 2019 from 15:17:00-15:18:28. a) Mobile platform measurements of 15-sec averaged CH_4 mole fractions (Receptor) downwind of Dairy III (Source). b) Methane flux footprint of Dairy III using the mobile survey shown in (a). The color gradient shows the relative contribution from the upwind areas where CH_4 was emitted. (c) Time series plot using 15-second averages from the mobile survey shown in (a). (d) Keeling plot using 15-second averages from the mobile survey shown in (a).

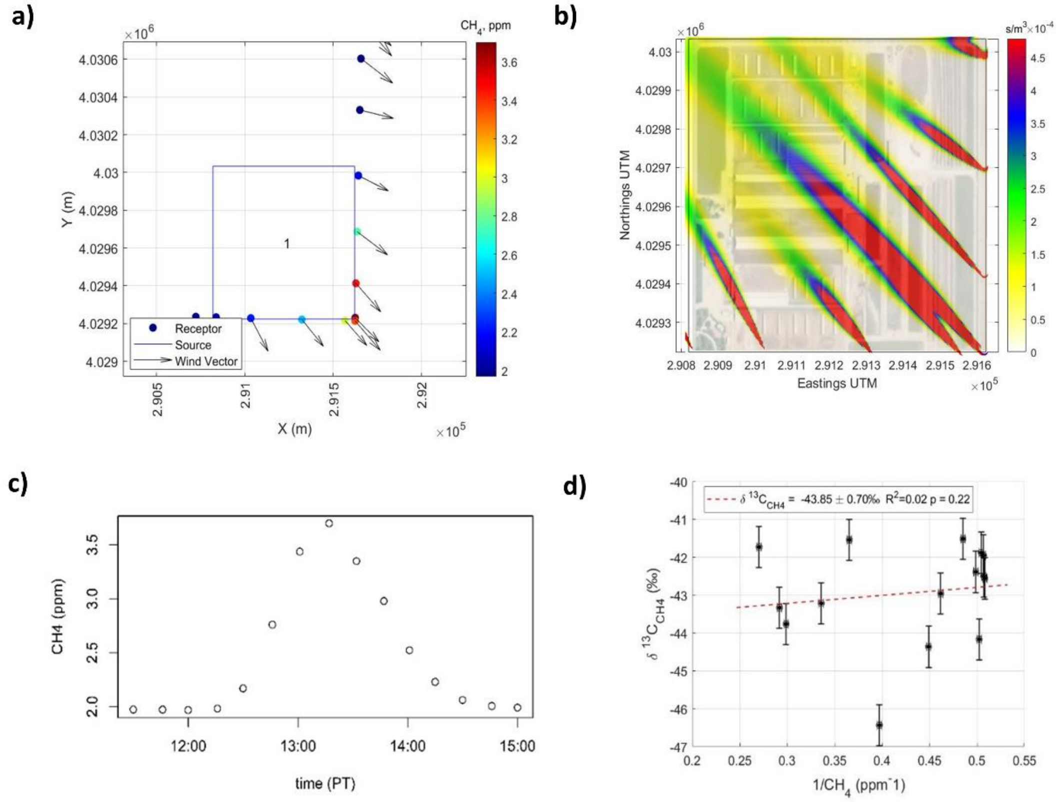

Figure S7. Isotopic signatures downwind of Dairy III on June 25th, 2019 from 17:11:30-17:15:00. a) Mobile platform measurements of 15-sec averaged CH_4 mole fractions (Receptor) downwind of Dairy III (Source). b) Methane flux footprint of Dairy III using the mobile survey shown in (a). The color gradient shows the relative contribution from the upwind areas where CH_4 was emitted. (c) Time series plot using 15-second averages from the mobile survey shown in (a). (d) Keeling plot using 15-second averages from the mobile survey shown in (a).

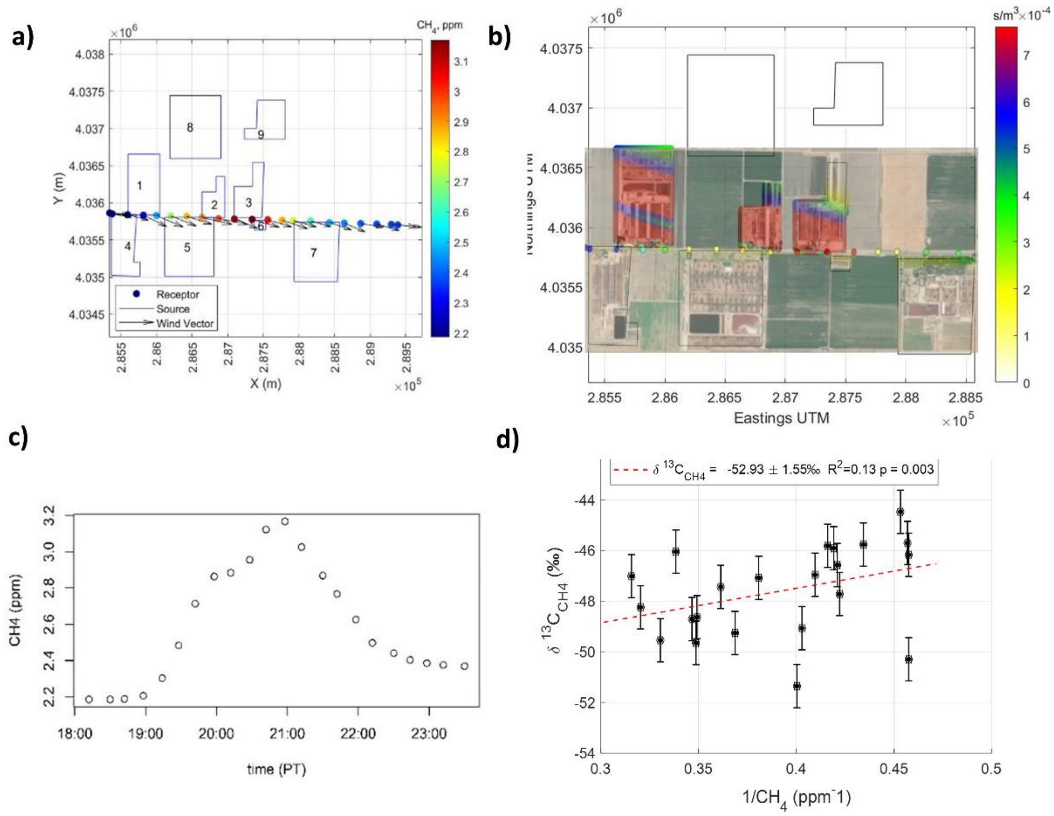

Figure S8. Isotopic signatures downwind of the Dairy Cluster on September 21st, 2018 from 17:18:12-17:23:36. a) Mobile platform measurements of 15-sec averaged CH_4 mole fractions (Receptor) downwind of the Dairy Cluster (Source). b) Methane flux footprints of the Dairy Cluster using the mobile survey shown in (a). The color gradient shows the relative contribution from the upwind areas where CH_4 was emitted. (c) Time series plot using 15-second averages from the mobile survey shown in (a). (d) Keeling plot using 15-second averages from the mobile survey shown in (a).

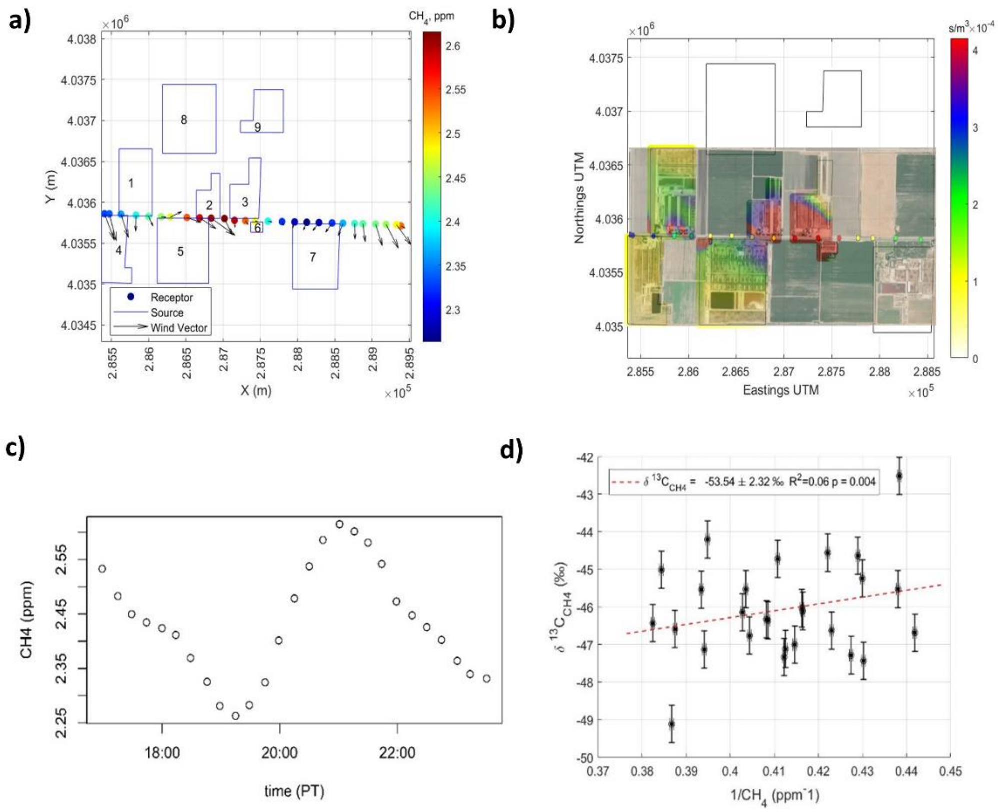

Figure S9. Isotopic signatures downwind of the Dairy Cluster on March 24th, 2019 from 14:16:59-14:23:34. a) Mobile platform measurements of 15-sec averaged CH_4 mole fractions (Receptor) downwind of the Dairy Cluster (Source). b) Methane flux footprints of the Dairy Cluster using the mobile survey shown in (a). The color gradient shows the relative contribution from the upwind areas where CH_4 was emitted. (c) Time series plot using 15-second averages from the mobile survey shown in (a). (d) Keeling plot using 15-second averages from the mobile survey shown in (a).

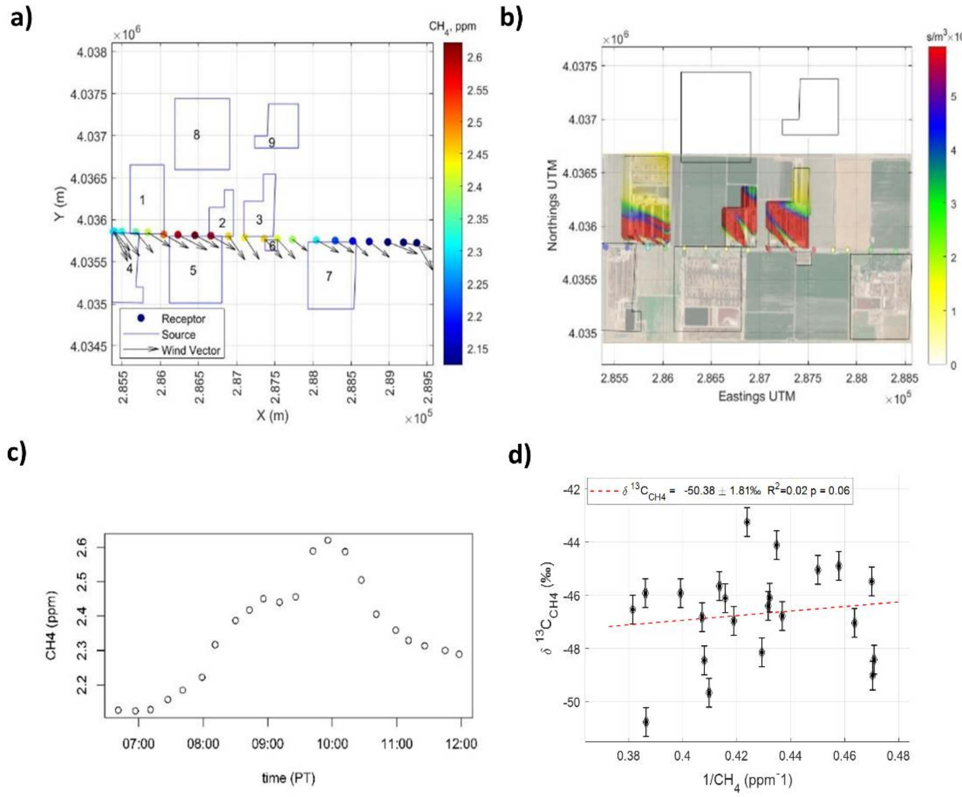

Figure S10. Isotopic signatures downwind of the Dairy Cluster on June 24th, 2019 from 16:06:41-16:12:05. a) Mobile platform measurements of 15-sec averaged CH_4 mole fractions (Receptor) downwind of the Dairy Cluster (Source). b) Methane flux footprints of the Dairy Cluster using the mobile survey shown in (a). The color gradient shows the relative contribution from the upwind areas where CH_4 was emitted. (c) Time series plot using 15-second averages from the mobile survey shown in (a). (d) Keeling plot using 15-second averages from the mobile survey shown in (a).

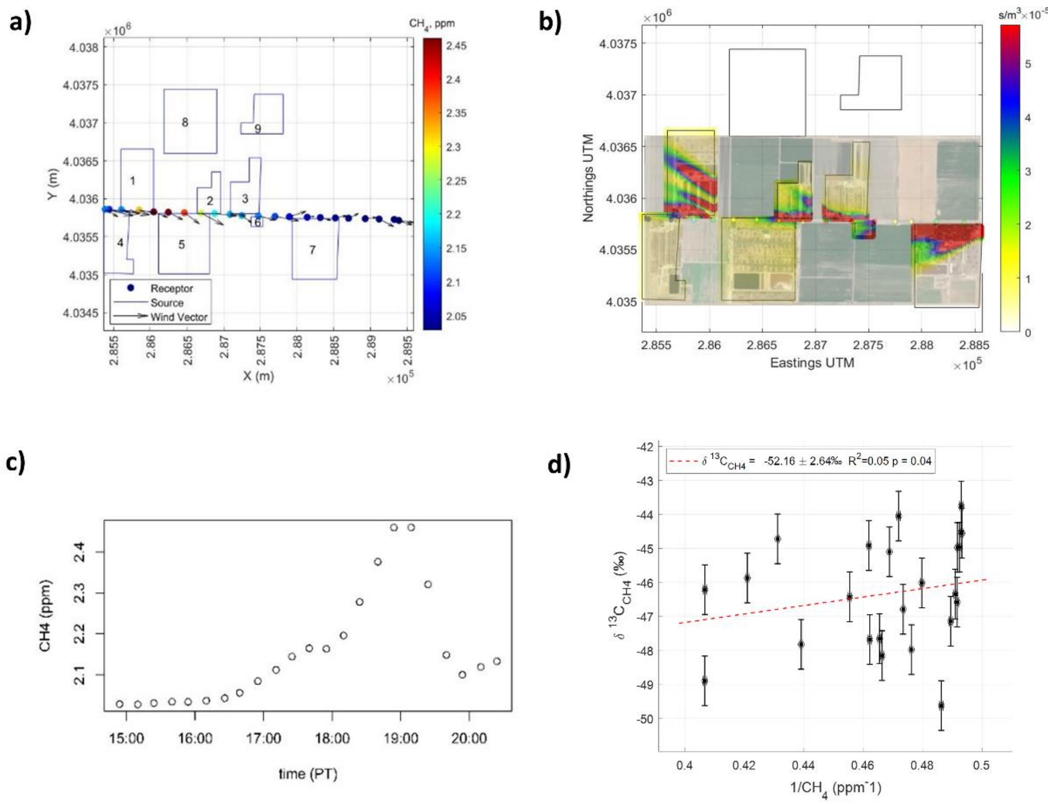

Figure S11. Isotopic signatures downwind of the Dairy Cluster on June 25th, 2019 from 14:14:54-14:20:28. a) Mobile platform measurements of 15-sec averaged CH_4 mole fractions (Receptor) downwind of the Dairy Cluster (Source). b) Methane flux footprints of the Dairy Cluster using the mobile survey shown in (a). The color gradient shows the relative contribution from the upwind areas where CH_4 was emitted. (c) Time series plot using 15-second averages from the mobile survey shown in (a). (d) Keeling plot using 15-second averages from the mobile survey shown in (a).